iScience

CellPress
OPEN ACCESS

Article

WLS-Wnt signaling promotes neuroendocrine prostate cancer

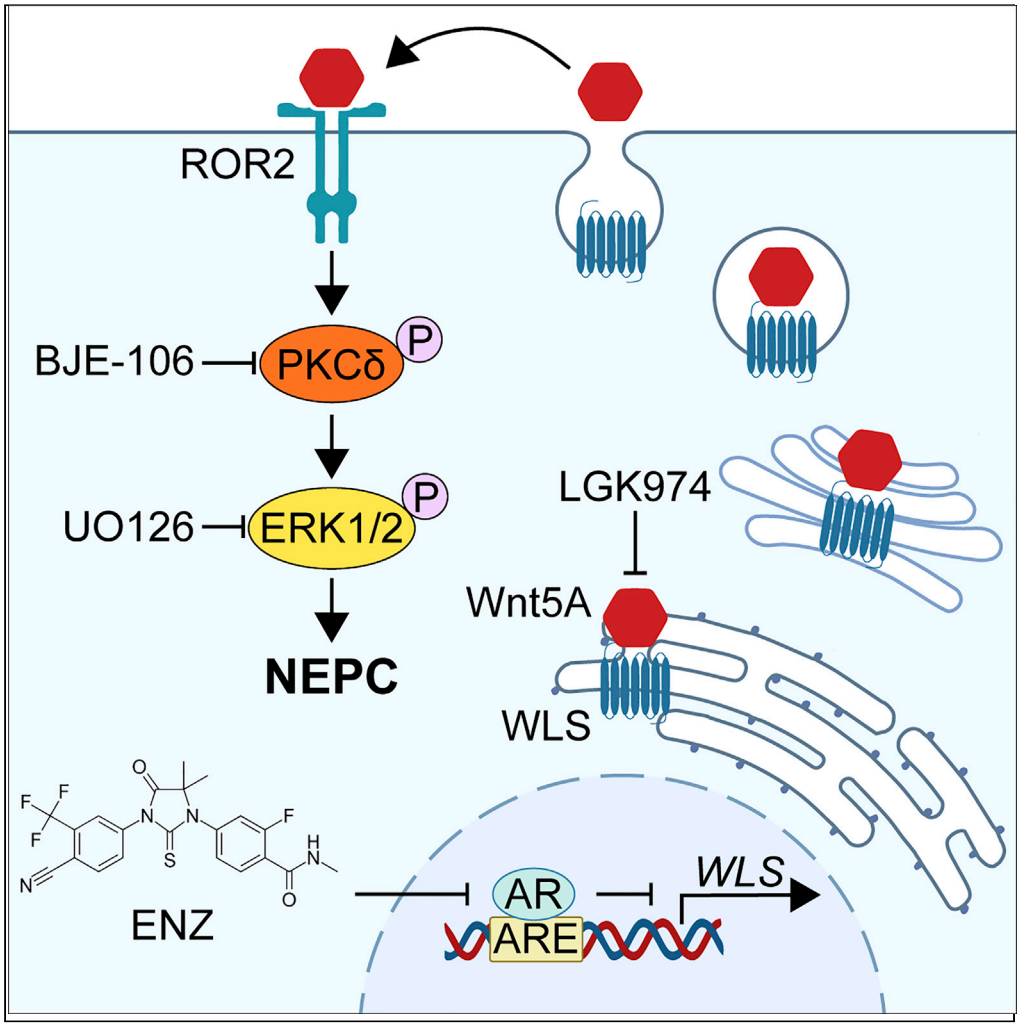

Tyler Bland, Jing Wang, Lijuan Yin, ..., Tzu-Ping Lin, Allen C. Gao, Boyang Jason Wu

boyang.wu@wsu.edu

Highlights

WLS is highly expressed in neuroendocrine prostate cancer clinical samples

WLS is a transcriptional target suppressed by androgen receptor

WLS drives neuroendocrine prostate cancer through the ROR2/PKCδ/ERK pathway

Wnt secretion inhibitor treatment limits neuroendocrine prostate tumor growth in mice

Bland et al., iScience 24, 101970
January 22, 2021
https://doi.org/10.1016/j.isci.2020.101970

iScience

CellPress
OPEN ACCESS

Article

WLS-Wnt signaling promotes neuroendocrine prostate cancer

Tyler Bland,[1,6] Jing Wang,[1] Lijuan Yin,[2] Tianjie Pu,[1] Jingjing Li,[1] Jin Gao,[1] Tzu-Ping Lin,[3,4] Allen C. Gao,[5] and Boyang Jason Wu[1,7,*]

Summary

Neuroendocrine prostate cancer (NEPC) is a lethal prostate cancer subtype arising as a consequence of more potent androgen receptor (AR) targeting in castration-resistant prostate cancer (CRPC). Its molecular pathogenesis remains elusive. Here, we report that the Wnt secretion mediator Wntless (WLS) is a major driver of NEPC and aggressive tumor growth *in vitro* and *in vivo*. Mechanistic studies showed that WLS is a transcriptional target suppressed by AR that activates the ROR2/PKCδ/ERK signaling pathway to support the neuroendocrine (NE) traits and proliferative capacity of NEPC cells. Analysis of clinical samples and datasets revealed that WLS was highly expressed in CRPC and NEPC tumors. Finally, treatment with the Wnt secretion inhibitor LGK974 restricted NE prostate tumor xenograft growth in mice. These findings collectively characterize the contribution of WLS to NEPC pathogenesis and suggest that WLS is a potential therapeutic target in NEPC.

Introduction

Prostate cancer (PC) is a current epidemic both globally and in the United States, with roughly 1 in 9 American men developing this disease during their lifetime (Siegel et al., 2019). Androgen deprivation therapy (ADT) is the standard of care, since dependence on androgen receptor (AR) signaling is a hallmark of PC. Although tumors initially respond, the disease eventually becomes resistant to ADT and progresses to the castration-resistant prostate cancer (CRPC) stage (Wong et al., 2014). Targeting the AR axis with more potent AR pathway inhibitors (APIs), including the second-generation AR antagonist enzalutamide (ENZ), has become a cornerstone therapeutic strategy for treating patients with CRPC (Sternberg, 2019). However, the clinical benefits are limited due to rapid development of drug resistance (Ramadan et al., 2015). The highly potent API-resistant CRPC variant is a significant clinical challenge. It can rapidly develop into a phenotype similar to lethal neuroendocrine prostate cancer (NEPC), characterized by neuroendocrine (NE) differentiated cell morphology and NE marker expression with reduced or lost reliance on AR (Beltran et al., 2014). Importantly, emerging evidence indicates that the incidence of this aggressive subtype of CRPC, also called treatment-induced NEPC (t-NEPC), has significantly increased in recent years due to the widespread use of highly potent APIs such as ENZ (Beltran et al., 2016). NEPC has been reported in up to 25% of patients with advanced treatment-resistant CRPC (Aparicio et al., 2011). However, the mechanisms by which CRPC transdifferentiates into NEPC are largely unknown. Currently, NEPC remains incurable with patient survival for less than a year following diagnosis (Wang et al., 2014). These dismal facts highlight the urgent need for a greater understanding of NEPC development and progression and new targeted therapies to improve survival.

Recently, accumulating evidence suggests that the Wnt signaling pathway plays a role in PC progression to an AR-indifferent or NE phenotype (Murillo-Garzon and Kypta, 2017). The Wnt proteins are secreted lipoglycoproteins with essential roles in regulating embryonic development, neuronal patterning, cell proliferation and migration, and axon guidance. There are 19 human Wnts regulating distinctive pathways via interaction with multiple cell surface receptors, including transmembrane frizzled (FZD) receptors, low-density lipoprotein receptor (LRP)4/5/6, receptor tyrosine kinase-like orphan receptor (ROR)1/2, and receptor-like tyrosine kinase. The major branches of Wnt pathways include the canonical pathway which utilizes β-catenin signaling (Wnt/β-catenin) and noncanonical pathways including planar cell polarity (Wnt/PCP) and calcium (Wnt/Ca^{2+}) signaling (Komiya and Habas, 2008). Multiple Wnts, including Wnt4, Wnt5A, Wnt7B, and Wnt11, and β-catenin signaling were shown to contribute to the development of API resistance

[1]Department of Pharmaceutical Sciences, College of Pharmacy and Pharmaceutical Sciences, Washington State University, Spokane, WA 99202, USA

[2]Uro-Oncology Research Program, Samuel Oschin Comprehensive Cancer Institute, Department of Medicine, Cedars-Sinai Medical Center, Los Angeles, CA 90048, USA

[3]Departmet of Urology, Taipei Veterans General Hospital, Taipei, Taiwan 11217, Republic of China

[4]Department of Urology, School of Medicine and Shu-Tien Urological Research Center, National Yang-Ming University, Taipei, Taiwan 11221, Republic of China

[5]Department of Urologic Surgery, University of California Davis, Sacramento, CA 95817, USA

[6]Present address: WWAMI Medical Education Program, University of Idaho, Moscow, ID 83844, USA

[7]Lead contact

*Correspondence: boyang.wu@wsu.edu

https://doi.org/10.1016/j.isci.2020.101970

in PC cells (Isaacsson Velho et al., 2020; Miyamoto et al., 2015; Zhang et al., 2018). Wnt7B and Wnt11 have been reported to induce NE differentiation and NE marker expression in PC cells (Moparthi et al., 2019; Uysal-Onganer et al., 2010). Since a large and varied number of Wnts, Wnt receptors, and Wnt-elicited signaling cascades are involved in API resistance and NE differentiation, targeting Wnt secretion instead of individual Wnts is likely to be a more promising way to block the entire Wnt signaling process in NEPC. Wnt secretion is mediated by the palmitoleation of most Wnts by *O*-acyltransferase porcupine (PORCN) in the ER. Palmitoleated Wnts are then transported to the cell surface for secretion by the carrier protein Wntless (WLS) (Yu et al., 2014). Recent evidence indicates that WLS promotes cellular resistance to ENZ in PC cells (Lombard et al., 2019), but WLS's function in NEPC remains to be elucidated.

Here, we investigated the role of WLS in NEPC emerging after prolonged API treatment. Using an *in vitro*-derived model of ENZ-resistant (ENZ^R) NEPC and data from PC patients, we show that WLS is transcriptionally repressed by AR, is required for NEPC growth and NE marker expression, and is highly expressed in human CRPC and NEPC. Mechanistically, silencing of WLS resulted in downregulation of the ROR2/PKCδ/ERK signaling cascade that is overexpressed in NEPC. These findings establish a functional role of WLS in the pathogenesis and progression of NEPC under the selective pressure of highly potent APIs like ENZ. Our results also identified WLS as a potential therapeutic target for this lethal form of PC.

Results

Wnt signaling and WLS expression are upregulated in ENZ^R NEPC cells

To model the clinical situation of CRPC transition to NEPC, we used an ENZ^R C4-2B ($C4\text{-}2B^{ENZR}$) cell line established by chronic exposure of human CRPC C4-2B cells to ENZ at gradually increasing doses to develop resistance (Liu et al., 2015). We performed expression profiling of $C4\text{-}2B^{ENZR}$ and control C4-2B cells. Gene set enrichment analysis (GSEA) demonstrated decreased expression of androgen-responsive genes, confirming the on-target molecular effects of ENZ even in resistant cells, with strong upregulation of neuronally expressed genes (Figure 1A). To minimize interference from acute ENZ treatment that may repress active AR expressed in ENZ^R cells, we next characterized $C4\text{-}2B^{ENZR}$ cells cultured in the absence of ENZ. NE markers such as CHGA and NSE showed enhanced expression in parallel to downregulated PSA expression in $C4\text{-}2B^{ENZR}$ cells compared to controls (Figure 1B). $C4\text{-}2B^{ENZR}$ cells also showed an NE differentiated cell morphology with an increase in per-cell number of neurites and average neurite length compared to control cells (Figures 1C and 1D). These results indicate the NE characteristics of $C4\text{-}2B^{ENZR}$ cells, recapitulating the progression of CRPC to NEPC under the pressure of ENZ.

In searching for potential pathway(s) driving the emergent NE phenotype of $C4\text{-}2B^{ENZR}$ cells, KEGG analysis revealed significant enrichment of the Wnt signaling pathway in $C4\text{-}2B^{ENZR}$ cells (Figure 1E), which coincides with the prevalent activation of most Wnts in $C4\text{-}2B^{ENZR}$ cells (Figure 1F). GSEA analysis also demonstrated several positively enriched gene signatures corresponding to Wnt-centric molecular events, including those related to both canonical and noncanonical Wnt signaling pathways, in $C4\text{-}2B^{ENZR}$ cells (Figures 1G and S1A), further supported by the observed upregulation of multiple genes engaged in either the canonical (*DKK1*, *LEF1* and *AXIN2*) or the noncanonical (*VANGL2*, *ROR2*, *WNT5A* and *DAAM2*) Wnt signaling pathways from our RNA-seq data (Figures S1B and S1C). These findings are consistent with the reported activation of both canonical and noncanonical Wnt signaling in ENZ^R PC cells (Chen et al., 2020; Zhang et al., 2018). Interestingly, the Wnt secretion mediator Wntless (*WLS*) was among the most upregulated Wnt-related genes in $C4\text{-}2B^{ENZR}$ cells compared to controls by RNA-seq (Figure S1B), further confirmed by a 6-fold increase of *WLS* mRNA level in $C4\text{-}2B^{ENZR}$ cells compared to controls by qPCR (Figure 1H). We also found higher WLS protein expression in whole cell lysates in parallel to more Wnt5A and Wnt11 proteins detected from conditioned media, reflecting their upregulation at the mRNA level, in $C4\text{-}2B^{ENZR}$ cells compared to controls (Figures 1I and S2). Together, these results suggest activated Wnt signaling and WLS expression in ENZ^R NEPC cells.

WLS is highly expressed in human CRPC and NEPC

To evaluate the clinical relevance of WLS in human CRPC and NEPC, we performed immunohistochemical (IHC) analysis of WLS expression in a tissue panel of hormone-sensitive PC (HSPC) and CRPC. We showed increased WLS protein expression in CRPC samples relative to HSPC counterparts (Figures 2A and 2B). We also demonstrated that WLS was co-expressed with the NE marker CHGA at the per-cell staining level in the CRPC cohort (Figures 2C and 2D). Next, we assessed *WLS* expression in RNA-seq data from CRPC and NEPC patient tumors using publicly available datasets. Analyzing the Beltran cohorts, we showed

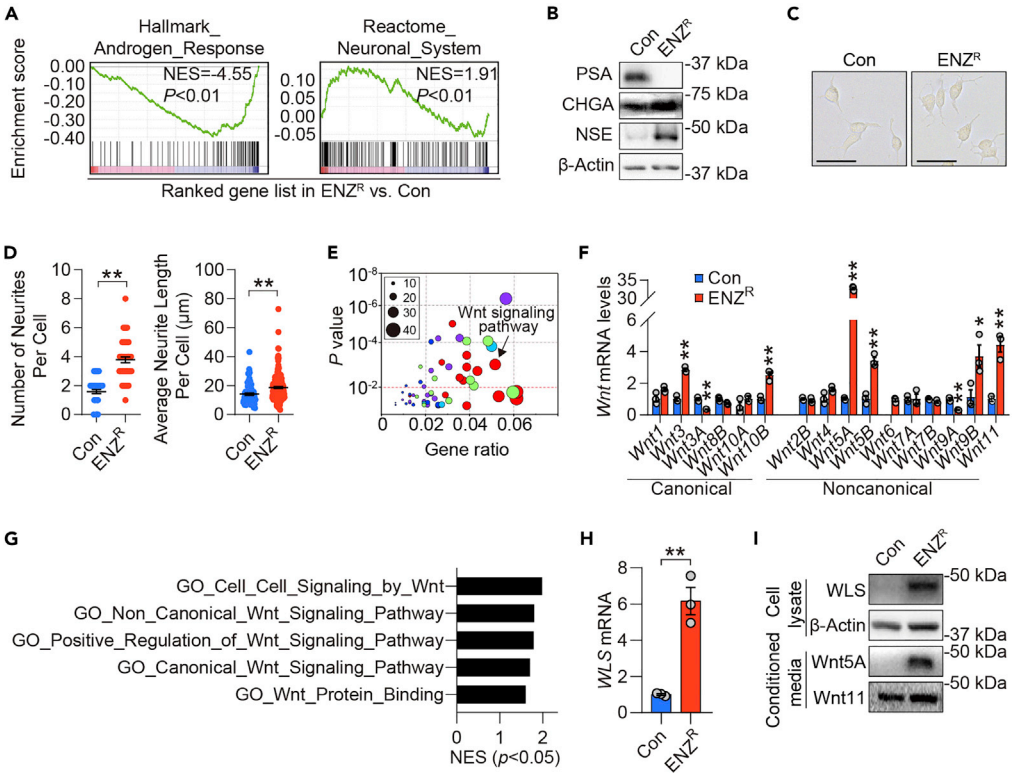

Figure 1. Wnt signaling and WLS expression are upregulated in ENZ^R NEPC cells

(A) GSEA plots of enrichment of gene signatures related to androgen response and neuronal system in ENZ^R C4-2B (C4-2B^{ENZR}) cells compared to ENZ-sensitive control C4-2B cells.

(B) Western blot analysis of PSA, CHGA, and NSE protein expression in control and ENZ^R C4-2B cells.

(C) Representative images of control and ENZ^R C4-2B cell morphology. Scale bars: 50 μm.

(D) Quantification of per-cell number of neurites and average neurite length in control and ENZ^R C4-2B cells (n = 50 cells per cell line), which is shown as a representative of 3 independent experiments. Data represent the mean ± SEM. **p < 0.01, unpaired *t* test.

(E) KEGG pathway analysis of the top 57 pathways upregulated in ENZ^R C4-2B cells compared to controls. KEGG pathways were clustered based on functional relation, indicated by different colors (red, signal transduction; green, human diseases; light blue, cellular processes; dark blue, metabolism; purple, organismal systems). The Wnt signaling pathway is pointed out by an arrow.

(F) RT-qPCR analysis of *Wnt* gene expression categorized based on the ability to activate the canonical or noncanonical Wnt signaling pathways in control and ENZ^R C4-2B cells (n = 3). Data represent the mean ± SEM. *p < 0.05, **p < 0.01, unpaired *t* test.

(G) GSEA analysis of select positively enriched Wnt-related gene sets in C4-2B^{ENZR} cells compared to controls.

(H) RT-qPCR analysis of *WLS* mRNA expression in control and ENZ^R C4-2B cells (n = 3). Data represent the mean ± SEM. **p < 0.01, unpaired *t* test.

(I) Western blot analysis of WLS protein expression in cell lysates and secreted Wnt5A and Wnt11 protein levels in conditioned media of control and ENZ^R C4-2B cells.

See also Figures S1 and S2.

significant activation of *WLS* transcript in NEPC tumors, classified by NE histomorphology and an integrated NEPC score based on a set of 70 NE reference genes (Beltran et al., 2016), compared with CRPC (Figure 2E). Similarly, we revealed an upward trend of *WLS* mRNA levels in NEPC compared to CRPC in 2 additional independent datasets (Figure S3). Moreover, *WLS* demonstrated a significant positive co-expression correlation with multiple canonical NE marker genes and an inverse relationship with *REST*, a transcription factor lost during progression to NEPC (Lapuk et al., 2012), at the mRNA level in the Beltran dataset (Figure 2F). Further, we found a rise of normalized *WLS* and *CHGA* transcript levels toward an increasing degree of NE differentiation in a panel of human PC cell lines, with a roughly 2-fold increase for both genes in the NEPC tumor-derived NCI-H660 cell line compared to the AR-dependent, non-NEPC LNCaP cell line, by interrogating a human PC cell line RNA-seq database (Figure 2G) (Lee et al.,

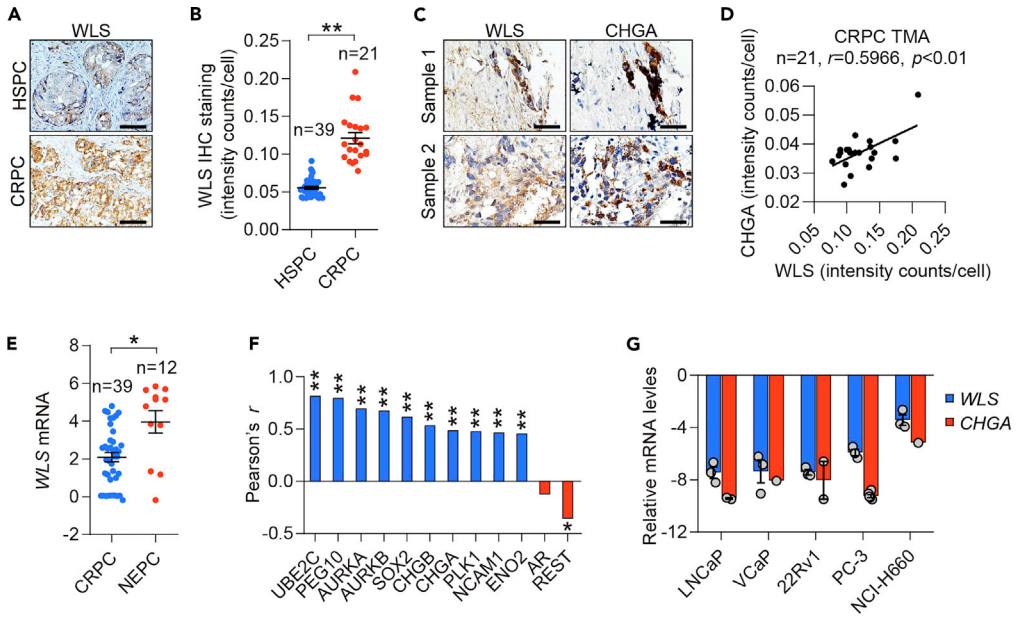

Figure 2. WLS is highly expressed in human CRPC and NEPC

(A) IHC images of WLS protein expression in representative CRPC versus hormone-sensitive counterpart (HSPC) patient samples from the cohorts described in (B). Scale bars: 20 μm.

(B) Quantification of WLS protein expression between HSPC (n = 39) and CRPC (n = 21) cohorts by average cell-based IHC staining intensity counts analyzed by inForm software. Data represent the mean ± SEM. **p < 0.01, unpaired *t* test.

(C) IHC images of WLS and CHGA protein staining in two representative CRPC patient samples. Scale bars: 20 μm.

(D) Protein co-expression correlation between WLS and CHGA in the CRPC cohort (n = 21). Average cell-based staining intensity counts for each individual protein were analyzed by inForm software to access the co-expression correlation by Pearson correlation.

(E) Quantification of *WLS* mRNA expression between CRPC (n = 39) and NEPC (n = 12) cohorts in the Beltran dataset. Data represent the mean ± SEM. *p < 0.05, unpaired *t* test.

(F) mRNA co-expression correlation of *WLS* with NE marker genes, *AR* and *REST* represented by positive (blue) or inverse (red) correlations in the Beltran dataset. *p < 0.05, **p < 0.01, Pearson correlation.

(G) Relative *WLS* and *CHGA* mRNA levels normalized to *ACTB* in human PC cell lines toward an increasing degree of NE differentiation from CellExpress.

See also Figure S3.

2018b). These data in aggregate demonstrate that WLS expression is strongly associated with PC disease severity, especially the NE phenotype, in a clinical setting.

WLS is transcriptionally repressed by AR

Since one of the defined features of NEPC is attenuated AR signaling, we examined the possibility that inhibition of the AR pathway increases the expression of WLS in NEPC. Growing AR-positive, androgen-sensitive LNCaP and C4-2B cells in media supplemented with charcoal-stripped serum (CSS) to remove androgens resulted in a marked increase in WLS protein expression that was reversed by treatment with the synthetic androgen R1881 (Figure 3A). Treatment of LNCaP cells with ENZ also time-dependently induced WLS protein expression (Figure 3B). To determine the direct effect of AR on WLS, siRNA-mediated silencing of AR, accompanied by reduced PSA protein expression, increased WLS protein levels under both androgen-depleted and -replete conditions in LNCaP and C4-2B cells (Figure 3C). Moreover, we showed that R1881 treatment suppressed *WLS* mRNA level by 48% in LNCaP cells (Figure 3D), which was corroborated by an up to 10-fold increase of *WLS* transcript level in LNCaP cells in response to CSS media over long-term culture within a period time of 12 months (Figure 3E). This suggests that *WLS* expression might be repressed by AR at the transcriptional level.

To determine whether AR directly binds to the *WLS* gene locus to mediate its transcriptional repression, we analyzed two chromatin immunoprecipitation (ChIP)-seq datasets involving subjects from both cultured human PC cells and clinical prostate tumors. We found AR enrichment at two distinct sites upstream

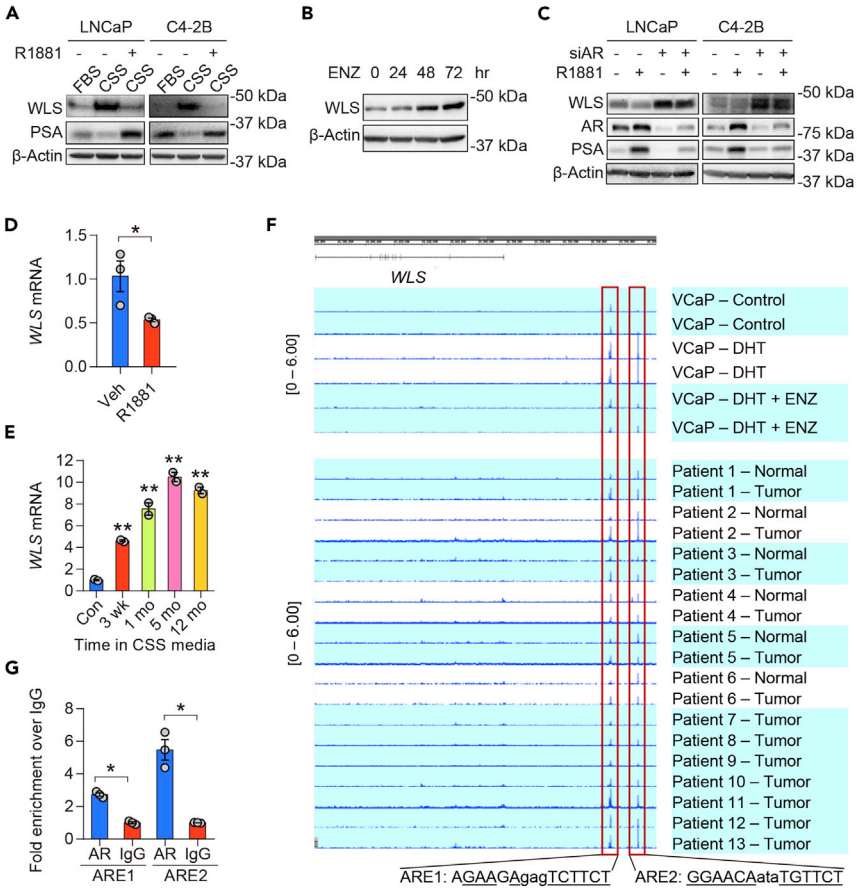

Figure 3. *WLS* is directly transcriptionally repressed by AR

(A) Western blot analysis of WLS and PSA protein expression in LNCaP and C4-2B cells grown in normal growth media (FBS, 5 days), CSS media (5 days), or CSS media (2 days) followed by R1881 treatment (1 nM, 72 hr).

(B) Western blot analysis of WLS protein expression in LNCaP cells grown in normal media treated with 20 μM ENZ for different times.

(C) Western blot analysis of WLS protein expression in LNCaP and C4-2B cells transfected with a scrambled siRNA or siRNA against *AR* (siAR) for 48 hr prior to treatment with either CSS media or CSS media supplemented with 1 nM R1881 for additional 72 hr.

(D) RT-qPCR analysis of *WLS* mRNA levels in LNCaP cells grown in CSS media for 48 hr followed by treatment with or without 1 nM R1881, with ethanol as a vehicle (Veh), for additional 72 hr (n = 3). Data represent the mean ± SEM. *$p < 0.05$, unpaired *t* test.

(E) Relative *WLS* mRNA expression in LNCaP cells exposed to long-term culture in CSS media measured by RNA-seq from dataset GSE8702. Data represent the mean ± SEM. **$p < 0.01$, one-way ANOVA.

(F) Genomic browser representation of AR binding in the distal enhancer region of *WLS* gene from VCaP cells and PC patient samples extracted from ChIP-seq datasets GSE55062 and GSE70079, respectively. Each track depicts ChIP-seq AR binding intensity for a given sample. The sequences of androgen response element (ARE) at each locus are shown with nucleotides homologous to the canonical ARE underlined.

(G) ChIP-qPCR assays of AR occupancy of two ARE-centric enhancers of *WLS* gene (n = 3). Data represent the mean ± SEM. *$p < 0.05$, unpaired *t* test.

See also Figure S4.

from the transcription start site (TSS) of *WLS* across the majority of samples examined. In the AR-expressed, androgen-sensitive VCaP cells, the affinity of AR association with the *WLS* gene locus was enhanced under androgen treatment, which was repressed in response to ENZ. In the human samples, AR was shown to be able to interact with the two regions of *WLS* genomic sequences in both tumor and adjacent normal prostate tissues from 6 matched pairs of samples, where the majority of samples demonstrated visibly higher AR occupancy in at least one region if not both in tumors versus in normal tissues. Of note, AR was found present at the *WLS* gene locus with varied levels of binding in all 13 human tumors included in the ChIP-seq

dataset. Further, we identified two consensus androgen response elements (AREs), AGAAGAgagTGTTCT and GGAACAataTGTTCT (−75631∼-75645 and −95,081∼-95095, respectively, with *WLS* TSS set as +1), which both have high homology (10 of 12 bp and 12 of 12 bp for ARE1 and ARE2, respectively) with the canonical sequence GGT/AACAnnnTGTTCT for AR binding (Figure 3F) (Roche et al., 1992). We conducted ChIP assays coupled with quantitative PCR using primers that amplified the putative AR-binding sites and detected significant AR enrichment at the two ARE-centric regions in LNCaP cells after R1881 stimulation (Figure 3G). We also examined whether AR-V7, a constitutively active AR splice variant that was negligibly expressed in the parental C4-2B cells but highly induced in C4-2B^{ENZR} cells after prolonged ENZ treatment (Liu et al., 2018), interacts with the *WLS* gene locus by interrogating a ChIP-seq dataset seeking the AR-V7 association with chromatin in the CRPC LN95 cell line. We identified a putative site upstream from the TSS of *WLS* as likely for AR-V7 binding, which was distinct from the 2 sites validated for full-length AR binding, but we did not find any consensus AREs possessing a high sequence similarity with the canonical one in the AR-V7-occupied sequences (Figure S4). Thus, we reasoned that AR-V7 might not contribute directly to transcriptional regulation of *WLS* in PC cells. Collectively, these results suggest that WLS is negatively regulated by AR, possibly through direct AR binding to two AREs in the *WLS* enhancer region.

WLS is required for NEPC cell growth and NE marker expression

Our data suggest that WLS activation coevolves with the emergence of ENZ-induced NE differentiation in CRPC. To assess the requirement for WLS in supporting an NE phenotype in ENZ^{R} cells, we stably knocked down WLS expression using two shRNAs targeting separate, non-overlapping *WLS* coding regions in C4-2B^{ENZR} cells, which was confirmed by reduced protein levels of WLS and Wnt5A in cell lysates and conditioned media, respectively, as compared to controls by Western blot analysis (Figure 4A). We found that WLS knockdown (KD) yielded a marked reduction in the protein expression levels of two NE markers, NSE and CD56, in C4-2B^{ENZR} cells compared to controls (Figure 4A). Consistently, treatment of C4-2B^{ENZR} cells with LGK974, a small-molecule PORCN inhibitor blocking Wnt secretion and currently under a phase I clinical cancer therapy trial (NCT01351103) (Liu et al., 2013), also decreased the protein expression levels of NSE and CD56 in a dose-dependent manner. The successful blockade of Wnt secretion by LGK974 was confirmed by the absence of Wnt5A detection in the conditioned media of ENZ^{R} cells (Figure 4B). Moreover, we showed that addition of recombinant Wnt5A protein rescued the suppressive effect of WLS silencing on expression of the NE marker CD56 (Figure 4C), suggesting that WLS's effect on NE markers may be mediated by secretion of Wnt proteins. In addition to the expression of terminal NE markers, we also sought to determine if WLS is important in regulating the aggressive behavior of NEPC. We investigated the effects of WLS KD on the proliferation of three NE or NE-like PC cell lines, C4-2B^{ENZR}, 22Rv1 and PC-3. The 22Rv1 cell line was derived from a human prostate adenocarcinoma xenograft displaying an NE phenotype (Huss et al., 2004; Sramkoski et al., 1999), and showed upregulation of NE markers such as NSE under hypoxia or combined androgen deprivation and ENZ treatment (Lee et al., 2019; Qi et al., 2010). The 22Rv1 cell line also expresses AR and AR splice variants rendering cells resistant to ENZ (Li et al., 2013). Thus, the 22Rv1 cell line may well represent a clinically observed amphicrine phenotype of PC, classified as tumors composed of cells co-expressing AR and NE genes (Labrecque et al., 2019). The NE-like PC-3 cell line is AR negative with characteristics of prostatic small cell NE carcinoma and has been utilized in several NEPC studies (Guo et al., 2019; Tai et al., 2011). We showed that WLS KD significantly reduced proliferation and colony formation in all cell lines (Figures 4D, 4E, and S5), which expands the findings of reduced colony formation in C4-2B^{ENZR} and 22Rv1 cells after WLS silencing from a recent study (Lombard et al., 2019). Intriguingly, WLS KD also produced decreases of proliferation and colony formation seen in parental C4-2B cells to a similar extent in C4-2B^{ENZR} cells, suggesting that WLS might be indispensable for growth of PC cells regardless of their NE state (Figure S5). In addition, LGK974 treatment dose-dependently inhibited the proliferation of both C4-2B^{ENZR} and 22Rv1 cells (Figure 4F). These results indicate that WLS is essential for NE differentiation and NEPC cell growth.

WLS induces NEPC through the ROR2/PKCδ/ERK pathway

To investigate the mechanism that mediates WLS's effect in NEPC, we first examined canonical Wnt/β-catenin pathway activity in C4-2B^{ENZR} cells. We showed increased phosphorylation levels of LRP6 in C4-2B^{ENZR} cells compared to controls (Figure S6A), an early step during activation of the canonical Wnt/β-catenin pathway (Tamai et al., 2004), which is consistent with findings from a recent report using the same ENZ^{R} cells as this study (Lombard et al., 2019). We further found marginally more accumulation of β-catenin protein in the nucleus of C4-2B^{ENZR} cells compared to controls, accompanied by higher β-catenin transcriptional activity reflected by a slight increase of TOPFlash luciferase activity after normalization with FOPFlash

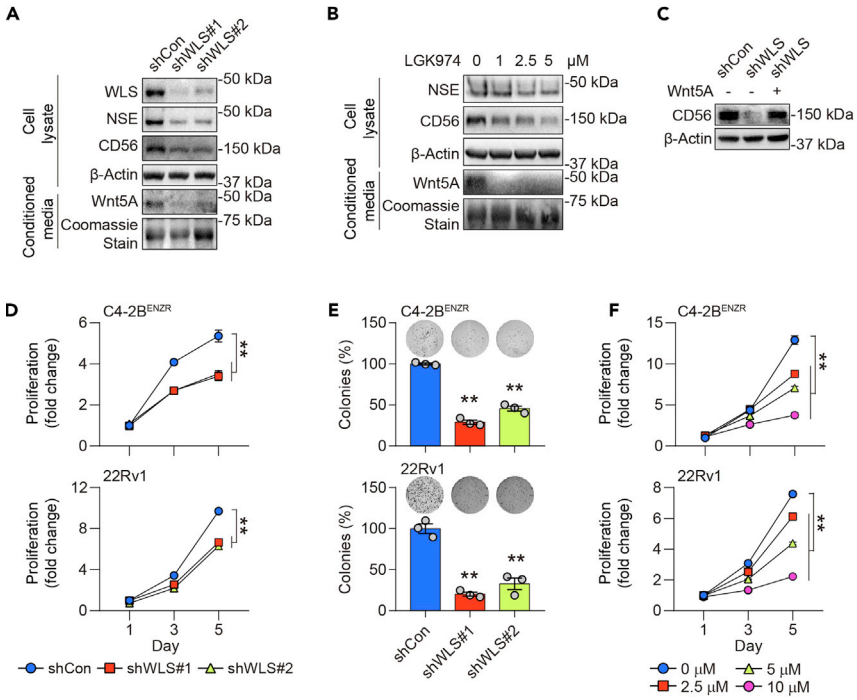

Figure 4. WLS is required for NEPC cell growth and NE marker expression

(A) Western blot analysis of WLS, NSE and CD56 protein expression and Wnt5A secretion in lysates or conditioned media of control (shCon) and WLS-KD (shWLS) C4-2B^{ENZR} cells.

(B) Western blot analysis of NSE and CD56 protein expression and Wnt5A secretion in C4-2B^{ENZR} cells treated with LGK974 at different concentrations for 7 days.

(C) Western blot analysis of CD56 protein expression in control, WLS-KD and WLS-KD/recombinant Wnt5A protein-added (100 ng/mL, 3 days) C4-2B^{ENZR} cells.

(D) Proliferation curves of control and WLS-KD C4-2B^{ENZR} and 22Rv1 cells by crystal violet staining (n = 4). Data represent the mean ± SEM. **p < 0.01, one-way ANOVA.

(E) Colony formation assays of control and WLS-KD C4-2B^{ENZR} and 22Rv1 cells (n = 3) with the number of colonies in respective control groups set as 100%. Representative images from each group are shown. Data represent the mean ± SEM. **p < 0.01, one-way ANOVA.

(F) Proliferation curves of C4-2B^{ENZR} and 22Rv1 cells treated with LGK974 at different concentrations by crystal violet staining (n = 4). Data represent the mean ± SEM. **p < 0.01, one-way ANOVA.

See also Figure S5.

activity (Figures S6B and S6C). Since these results indicating very little upregulation of β-catenin did not conform to substantial activation of WLS in C4-2B^{ENZR} cells, we reasoned that the canonical Wnt/β-catenin pathway might play a minor role mediating WLS's effect in ENZ-induced NEPC.

Next, we questioned whether the noncanonical Wnt pathway involving multiple intracellular signaling cascades possibly provides a major avenue for WLS's function in NEPC. We performed an unbiased proteomic screen using a Wnt signaling phospho antibody array featuring 227 site-specific and phospho-specific antibodies important to the Wnt pathway. The levels of signaling proteins were compared in WLS-KD and control C4-2B^{ENZR} cells. Intriguingly, the screen revealed that several phosphoproteins essential in the noncanonical Wnt pathway, such as PKCδ, JNK, and AKT, were downregulated by WLS silencing compared to controls. PKCδ stands out from the list of candidate phosphoproteins because it has the most phosphorylation sites (Y64, Y313, T505, and S645) affected by WLS inhibition (Figure 5A). We validated the decline in phosphorylation levels of PKCδ protein in WLS-KD C4-2B^{ENZR} cells compared to controls (Figure 5B), with negligible changes in phosphoprotein levels of either JNK or AKT (Figure S7A). Using a candidate approach to search for effector molecule(s) downstream of PKCδ, we showed a reduction in phosphorylated ERK protein levels in WLS-KD C4-2B^{ENZR} cells compared to controls (Figure 5B). The MAPK/ERK pathway was previously demonstrated to be involved in acquiring NE properties in PC and non–small cell lung cancer cells (Chen et al., 2014; Kim et al., 2002, 2017). Consistent with observed WLS activation,

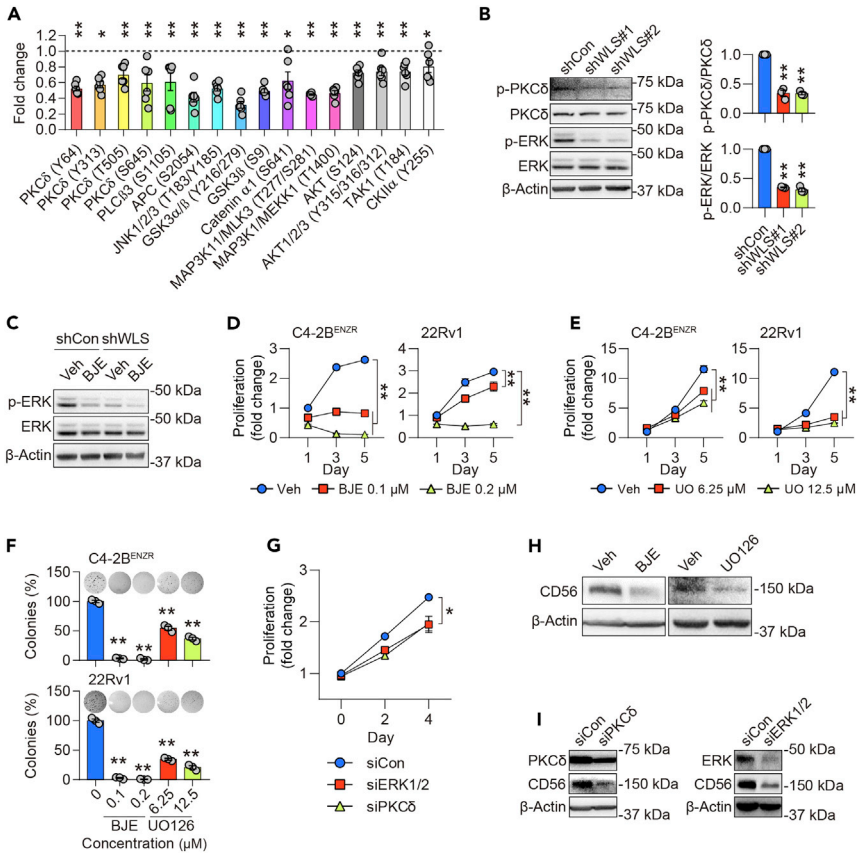

Figure 5. WLS mediates NEPC cell growth through the PKCδ/ERK pathway

(A) Phospho antibody array analysis of phosphoproteins implicated in Wnt signaling in WLS-KD C4-2B^{ENZR} cells. All phosphoproteins with significantly ($p < 0.05$) decreased levels in WLS-KD cells compared to controls are presented. All phospho signals were normalized to their total forms from a single array with 6 replicate spots (n = 6). Data represent the mean ± SEM. *$p < 0.05$, **$p < 0.01$, unpaired *t* test.

(B) Western blot analysis of p-PKCδ, PKCδ, p-ERK and ERK protein expression in control and WLS-KD C4-2B^{ENZR} cells, with quantification of normalized p-PKCδ and p-ERK levels presented separately (n = 3). Data represent the mean ± SEM. **$p < 0.01$, unpaired *t* test.

(C) Western blot analysis of p-ERK and ERK protein expression in control and WLS-KD C4-2B^{ENZR} cells treated with BJE-106 (BJE, 0.1 μM, 3 hr).

(D and E) Proliferation curves of C4-2B^{ENZR} and 22Rv1 cells treated with BJE-106 (D) or UO126 (UO, E) at different concentrations by crystal violet staining (n = 4). Data represent the mean ± SEM. **$p < 0.01$, one-way ANOVA.

(F) Colony formation assays of C4-2B^{ENZR} and 22Rv1 cells treated with BJE-106 or UO126 at different concentrations (n = 3). Representative images from each group are shown. Data represent the mean ± SEM. **$p < 0.01$, one-way ANOVA.

(G) Proliferation curves of C4-2B^{ENZR} cells treated with PKCδ or ERK1/2 siRNAs by MTS assays (n = 4). Data represent the mean ± SEM. *$p < 0.05$, unpaired *t* test.

(H) Western blot analysis of CD56 protein expression in C4-2B^{ENZR} cells treated by BJE-106 (0.1 μM, 7 days) or UO126 (6.25 μM, 7 days).

(I) Western blot analysis of CD56 protein expression in C4-2B^{ENZR} cells treated by PKCδ or ERK1/2 siRNAs.

See also Figures S6 and S7.

the protein expression levels of total PKCδ and both active p-PKCδ and p-ERK after normalization with respective controls were higher in C4-2B^{ENZR} cells relative to control cells (Figure S7B). Following a previous report of PKCδ activation of ERK in noncancerous cells (Ueda et al., 1996), treatment with BJE-106, a third-generation PKCδ inhibitor with a 1000-fold selectivity for PKCδ over PKCα (Takashima et al., 2014), lessened ERK protein phosphorylation in C4-2B^{ENZR} cells, reinforcing the idea that PKCδ regulates ERK in the NEPC context (Figure S7C). Moreover, we showed that BJE-106 treatment repressed active p-ERK protein levels in C4-2B^{ENZR} cells, with such repression visibly smaller after prior WLS KD, suggesting that WLS regulates ERK through PKCδ (Figure 5C). In addition, we demonstrated that inhibition of either

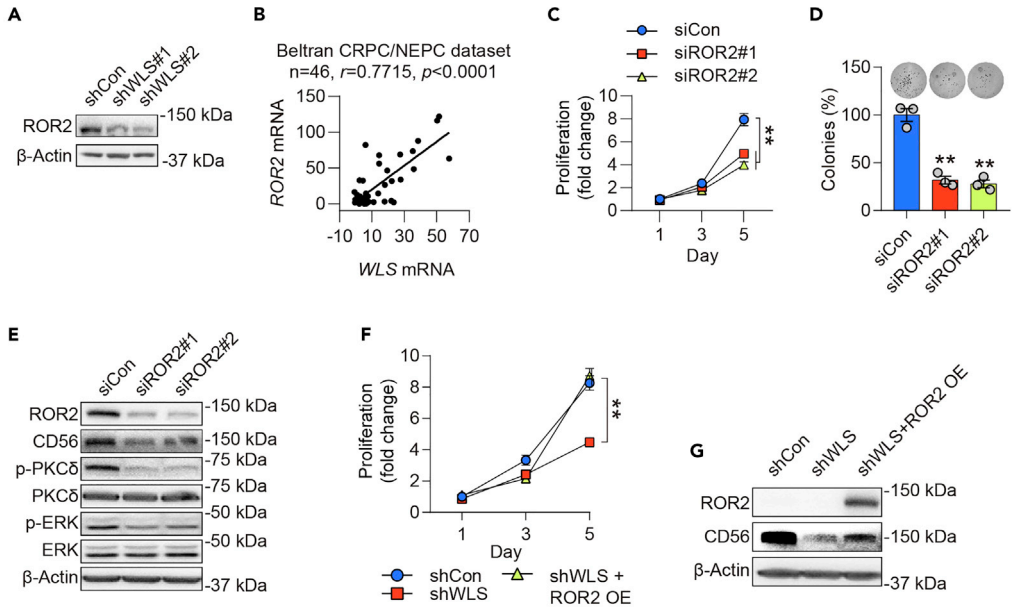

Figure 6. ROR2 mediates WLS induction of the PKCδ/ERK pathway

(A) Western blot analysis of ROR2 protein expression in control and WLS-KD C4-2B^{ENZR} cells.

(B) Co-expression correlation between *WLS* and *ROR2* mRNA in the Beltran dataset by Pearson correlation.

(C) Proliferation curves of C4-2B^{ENZR} cells treated with a scrambled siRNA (siCon) or *ROR2* siRNAs (siROR2) by crystal violet staining (n = 4). Data represent the mean ± SEM. **p < 0.01, one-way ANOVA.

(D) Colony formation assays of C4-2B^{ENZR} cells treated with a scrambled siRNA or *ROR2* siRNAs (n = 3). Data represent the mean ± SEM. **p < 0.01, one-way ANOVA.

(E) Western blot analysis of ROR2, CD56, p-PKCδ, PKC, p-ERK, and ERK protein expression in control and siRNA-mediated ROR2-KD C4-2B^{ENZR} cells.

(F) Proliferation curves of control, WLS-KD and WLS-KD/ROR2-overexpressing (OE) C4-2B^{ENZR} cells by crystal violet staining (n = 4). Data represent the mean ± SEM. **p < 0.01, one-way ANOVA.

(G) Western blot analysis of CD56 protein expression in control, WLS-KD and WLS-KD/ROR2-OE C4-2B^{ENZR} cells.

See also Figure S8.

PKCδ with BJE-106 or ERK with UO126, a highly selective inhibitor of MEK acting upstream of ERK, suppressed proliferation and colony formation of both C4-2B^{ENZR} and 22Rv1 cells in a dose-dependent manner (Figures 5D–5F), which was paralleled by a reduction of C4-2B^{ENZR} cell proliferation under treatment with PKCδ or ERK siRNAs (Figure 5G). Further analysis of terminal NE marker expression revealed that pharmacological or siRNA-mediated inhibition of PKCδ and ERK reduced CD56 protein levels in C4-2B^{ENZR} cells compared to controls (Figures 5H and 5I).

WLS transports Wnts intracellularly for secretion and subsequent interaction with a variety of cell surface receptors to elicit multiple signaling pathways. Seeking the main receptor mediating WLS-Wnt signaling in NEPC, we observed increased expression of *ROR2* from our RNA-seq data in C4-2B^{ENZR} cells (Figure S1B). ROR2, an orphan receptor tyrosine kinase, functions as a noncanonical Wnt receptor and binds Wnt5A, which was co-upregulated with *ROR2* in the C4-2B^{ENZR} transcriptome (Figure S1B) and reported to confer antiandrogen resistance in CRPC (Ho et al., 2012; Miyamoto et al., 2015). ROR2 has been shown to activate PKCδ and ERK in different cellular contexts (Cheung et al., 2011; Xu et al., 2017). Following initial findings from RNA-seq data, we showed increased ROR2 protein expression in C4-2B^{ENZR} cells compared to controls, which was recapitulated in parental LNCaP or C4-2B cells treated with CSS media or ENZ (Figures S8A–S8C). Similar to *WLS*, *ROR2* was upregulated in human NEPC compared with CRPC from the Beltran cohorts, and demonstrated a significant positive co-expression correlation with multiple canonical NE marker genes along with an inverse relationship with *REST* and *AR* (Figures S8D and S8E). Interestingly, we found that ROR2 protein expression was repressed when WLS was knocked down in C4-2B^{ENZR} cells (Figure 6A), supported by a positive *WLS-ROR2* co-expression correlation from the Beltran CRPC/NEPC dataset (Figure 6B). Silencing of ROR2 inhibited proliferation and colony formation of C4-2B^{ENZR} cells, accompanied by reduced protein levels of CD56, p-PKCδ and p-ERK (Figures 6C–6E). We further

demonstrated that transient forced expression of ROR2 reverted the suppression of proliferation and CD56 protein expression caused by WLS silencing in C4-2B^{ENZR} cells (Figures 6F and 6G), indicating ROR2's ability to overcome the effect of Wnt secretion blockade and thus rescue the NEPC phenotype. Overall, these data support the idea that WLS induces NEPC through the ROR2-dependent PKCδ/ERK pathway.

WLS silencing inhibits NEPC tumor growth

To determine if the reduced proliferative capacity of WLS-silenced NEPC cells *in vitro* could be translated *in vivo*, we used 22Rv1 cells to establish subcutaneous xenograft tumors in castrated mice. We demonstrated a significant reduction in tumor growth rate and tumor weight when WLS was knocked down in tumors compared to the control group (Figures 7A and 7B). IHC analysis of tumor samples revealed lowered WLS protein expression in WLS-KD tumors, indicating effective and sustainable WLS KD effect under *in vivo* conditions. A 50% decrease of Ki-67^{+} cells, 25-fold higher cleaved caspase 3^{+} cells, and 63% lower CD34 staining intensity indicative of diminished tumor angiogenesis on average were found in WLS-KD tumors in comparison with controls. WLS silencing further reduced CD56, p-PKCδ, and p-ERK protein levels by an average of 30%, 26%, and 33% less staining intensity of respective proteins in WLS-KD tumors compared to controls (Figures 7C and 7D).

To test whether a Wnt secretion inhibitor could suppress NEPC growth *in vivo*, we inoculated castrated mice subcutaneously with 22Rv1 cells and treated them with LGK974 through oral daily administration. After we sacrificed the mice in the control group on day 14 due to their large tumors, we continued LGK974 treatment in the treatment group for another 7 days. The average tumor volume in mice receiving LGK974 treatment was 86% smaller than that in the control group (control group vs. LGK974-treated group: 1,841 $\pm$ 341 mm^3 vs. 327 $\pm$ 153 mm^3 on day 14, or 1,841 $\pm$ 341 mm^3 on day 14 vs. 249 $\pm$ 107 mm^3 on day 21) (Figure 7E). Consistently, LGK974 treatment resulted in a 71% reduction in tumor weight (control group vs. LGK974-treated group: 1.24 $\pm$ 0.28 g on day 14 vs. 0.36 $\pm$ 0.12 g on day 21) (Figures 7F and 7G). The efficacy of LGK974 for the blockade of Wnt secretion was confirmed by significantly less Wnt5A protein stained by IHC in tumors given LGK974 compared to controls. LGK974 treatment also yielded a 21% decrease of Ki-67^{+} tumor cells, a 7.5-fold increase of cleaved caspase 3^{+} tumor cells, and 44%, 71%, 35%, and 26% lower tumor expression of CD34, CD56, p-PKCδ, and p-ERK, respectively, compared to controls by IHC analysis (Figures 7H and 7I).

In summary, our preclinical studies using ENZ^{R} NEPC models revealed the prerequisite role of WLS in the development of an NE phenotype in CRPC. WLS is activated upon relieving AR transcriptional suppression and in turn activates the ROR2/PKCδ/ERK signaling pathway to promote NE marker expression and NEPC growth. This can be effectively limited by pharmacological inhibition of the Wnt secretion pathway mediated by WLS and its associated molecules.

Discussion

In this study, we identified WLS as an important mediator and potential therapeutic target in NEPC, a poorly understood and lethal disease which has shown increasing incidence in recent years after more potent APIs, including ENZ, began to be used for CRPC treatment. Our studies present several findings with implications for patients with CRPC and NEPC. Utilizing an *in vitro*-derived model of ENZ^{R} CRPC that faithfully mimics t-NEPC, we demonstrated that WLS, as activated in NEPC cells, is required for the NE and proliferative phenotype of NEPC cells. We also presented the evidence that WLS is suppressed by AR likely via direct AR interaction with 2 ARE-encompassing *WLS* enhancers, leading to WLS upregulation in NEPC cells where AR signaling in general is absent or inhibited. Further studies are warranted to validate the functionality of these AR-binding sites for modulating the transcription of *WLS*. Additionally, alternative mechanisms possibly contributing to WLS upregulation in NEPC cells, especially the reported Wnt ligand-dependent ERAD (endoplasmic reticulum-associated degradation) control of WLS protein levels based on the observed concurrent induction of WLS and Wnts in C4-2B^{ENZR} cells (Glaeser et al., 2018), also merit additional exploration. We further demonstrated the feasibility and efficacy of pharmacologically targeting Wnt secretion for inhibition of NEPC tumor growth in mice. These studies expand our understanding of the molecular pathogenesis of NEPC and provide a rationale for targeting Wnt secretion for the treatment and/or prevention of NEPC emerging from high-potency API-based CRPC therapy.

WLS is a Wnt cargo receptor protein first discovered in developmental biology in *Drosophila* and demonstrated in mammals later, where it serves as a core component of the Wnt secretion machinery to regulate

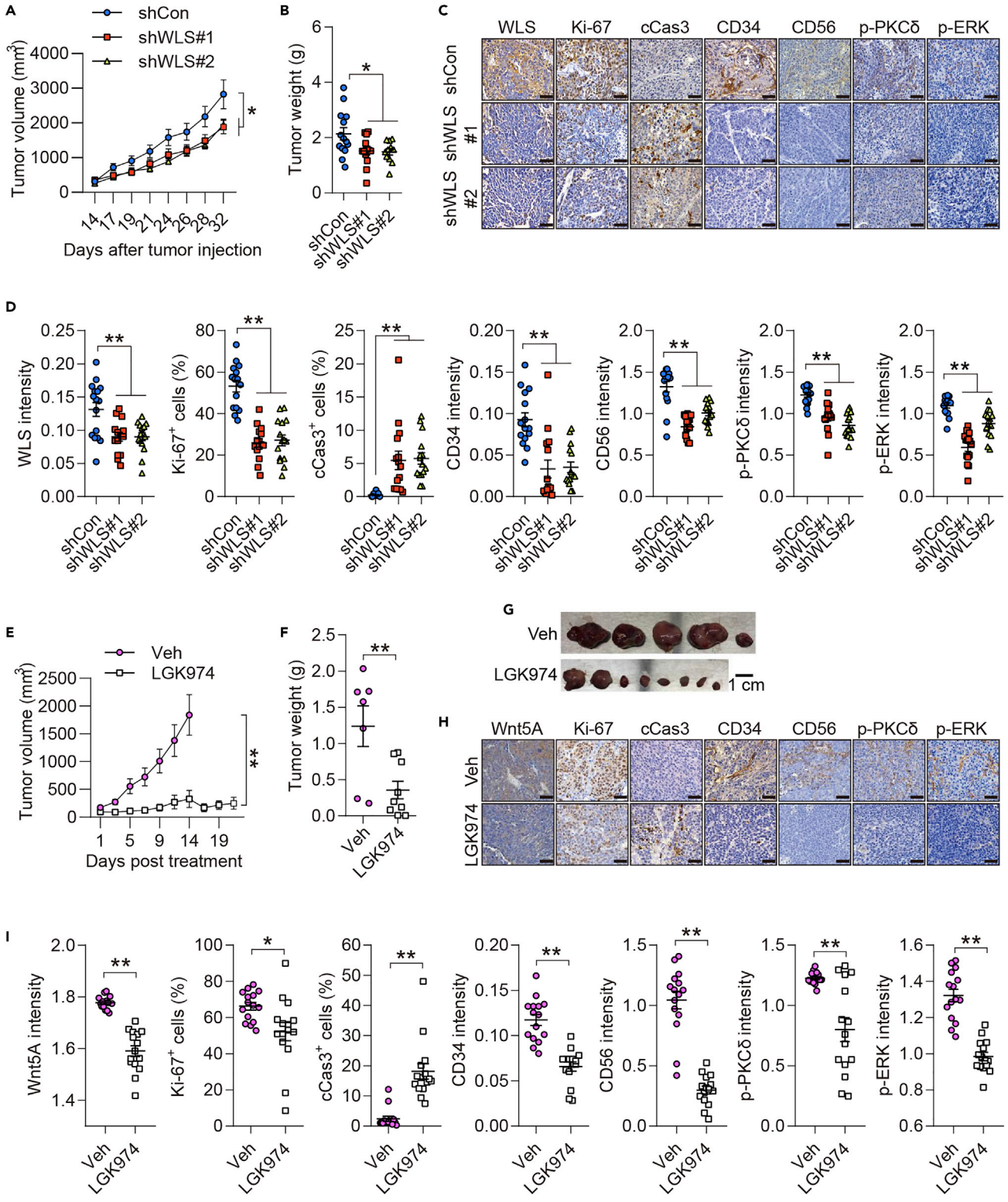

Figure 7. WLS silencing inhibits NEPC tumor growth in mice

(A) Growth curves of 22Rv1 tumors (shCon, n = 14; shWLS#1, n = 14; shWLS#2, n = 12) implanted subcutaneously in castrated SCID mice. Data represent the mean ± SEM. *p < 0.05, one-way ANOVA.

(B) Tumor weights measured for each group in (A) at the experimental endpoint. Data represent the mean ± SEM. *p < 0.05, one-way ANOVA.

Figure 7. *Continued*

(C) IHC representative images of WLS, Ki-67, cleaved caspase 3 (cCas3), CD34, CD56, p-PKCδ and p-ERK in tumor samples from each group in (A). Scale bars: 20 μm.

(D) Quantitation of WLS, CD34, CD56, p-PKCδ and p-ERK IHC per-cell staining intensity and % of Ki-67$^+$ or fold change of cCas3$^+$ cells in tumor samples from each group in (A) (n = 15). Data represent the mean ± SEM. **p < 0.01, one-way ANOVA.

(E) Growth curves of 22Rv1 subcutaneous tumors receiving corn oil (Veh, n = 7) or LGK974 (5 mg/kg, orally, n = 8) daily in castrated nude mice. Data represent the mean ± SEM. **p < 0.01, unpaired *t* test.

(F) Tumor weights measured for each group in (E) at respective experimental endpoints (Veh, day 14; LGK974, day 21). Data represent the mean ± SEM. **p < 0.01, unpaired *t* test.

(G) Anatomic images of tumors from each group in (E) at respective experimental end points.

(H) IHC representative images of WLS, Ki-67, cCas3, CD34, CD56, p-PKCδ and p-ERK staining in tumor samples from each group in (E). Scale bars: 20 μm.

(I) Quantitation of % of Ki-67$^+$ or fold change of cCas3$^+$ cells and CD34, CD56, p-PKCδ and p-ERK IHC per-cell staining intensity from each group in (E) (n = 15). Data represent the mean ± SEM. *p < 0.05, **p < 0.01, unpaired *t* test.

diverse processes including body axis formation, retinal angiogenesis, hair follicle formation, and bone mass regulation. WLS loss leads to intracellular accumulation of Wnts in Wnt-secreting cells without release of Wnts to the extracellular milieu, thereby impeding Wnt signaling (Banziger et al., 2006; Bartscherer et al., 2006; Fu et al., 2009; Goodman et al., 2006). Recent studies have brought WLS's role in cancer into focus owing to aberrant Wnt signaling molecularly linked to cancer development and progression. WLS has been shown to play a role in many human cancers, including glioma, bladder, gastric and colorectal cancers, and more recently PC (Augustin et al., 2012; Glaeser et al., 2018; Lombard et al., 2019; Schmid et al., 2017; Seo et al., 2018). Complementing these reports, we identified WLS as a highly expressed member of Wnt signaling from RNA-seq of an ENZ^R NEPC cell line, making it a top candidate for mediating NE differentiation in PC. Our observation of WLS upregulation in ENZ^R cells is also consistent with the findings from a recent study using the same ENZ^R cells as ours (Lombard et al., 2019). Mounting evidence suggests a conceptual two-stage progression to NEPC through the acquisition of an NE-like phenotype from an AR-dependent adenocarcinoma followed by the initiation of cell proliferation (Akamatsu et al., 2015). Our data indicate that WLS functions at both stages, because silencing WLS expression led to concomitant reduction in NE markers, NEPC cell proliferation, and NEPC tumor growth. In addition, our data from human specimens show the clinical relevance of WLS to aggressive PC, including CRPC and NEPC. The Beltran cohorts and 2 additional independent datasets showed that WLS tends to be increasingly expressed in clinically defined NEPC compared to CRPC tumors. In addition, WLS also has clinical relevance in PC beyond the NEPC context based on our observation of its overexpression in CRPC compared to HSPC in our cohorts. Using the same ENZ^R C4-2B cells as in our study, Lombard et al. recently showed that WLS silencing reduces expression of AR, AR variants, AR target genes and PSA levels in C4-2B^{ENZR} cells, and further restores ENZ sensitivity in resistant cells (Lombard et al., 2019). Coupling this report with our study, we argue that WLS may have the dual role of supporting the baseline activity and activation of AR signaling in AR-dominant PC disease stages, including CRPC, as well as heightening the potential for AR-suppressed NEPC disease progression in an androgen deprivation setting, which expands the therapeutic utility of targeting WLS for treatment of advanced PC, especially for the clinically emergent type of amphicrine tumors composed of cells exhibiting both AR and NE activity (Labrecque et al., 2019).

The transdifferentiation of CRPC into NEPC under selective pressure from APIs like ENZ requires activation of alternative survival pathways that replace AR as the driver of PC survival and growth. Our results show that inhibiting WLS suppresses a noncanonical Wnt pathway driven by the ROR2/PKCδ/ERK cascade, which is overexpressed in NEPC cells and is required for NE marker expression and NEPC cell growth. ROR2 is a favored receptor for Wnt5A to convey noncanonical Wnt5A signaling (Ho et al., 2012). *Wnt5A* is the most significantly activated Wnt from our RNA-seq data in ENZ^R NEPC cells, raising the possibility that Wnt5A is the dominant Wnt mediating WLS-Wnt signaling in NEPC. Wnt5A exhibits both tumor promoting and suppressive roles in PC, which likely depends on the combination and availability of different Wnt receptors for alterations in signaling output (Lee et al., 2018a; Ren et al., 2019; Thiele et al., 2018). We suspect that elevated expression of ROR2 in NEPC cells could release Wnt5A from association with other Wnt receptors, making it more prone to support NEPC growth. Intriguingly, we detected only a marginal increase of nuclear β-catenin level in parallel to much more WLS activation in ENZ^R cells, and therefore speculated that the canonical Wnt/β-catenin signaling might not play a principal role supporting WLS function in NEPC. On the other hand, using the same ENZ^R cells as ours, Lombard et al. recently showed that WLS silencing decreased canonical Wnt signaling evidenced by reduced levels of p-LRP6 and β-catenin target genes, including *LEF1* and *BAMBI*, but whether the canonical Wnt signaling directly mediates WLS's observed effect on cell behaviors was inconclusive in this study

(Lombard et al., 2019). Based on the findings of Lombard et al. and our findings, we argue that canonical and noncanonical Wnt signaling may both contribute to WLS's effects in ENZ^R NEPC, with the noncanonical Wnt signaling likely outcompeting the canonical signaling. Indeed, we revealed more drastic activation of noncanonical Wnts, such as Wnt5A, Wnt5B and Wnt11, as compared to canonical Wnts in ENZ^R cells. Further, these noncanonical Wnts including Wnt5A and Wnt11, which both are concomitantly implicated in NEPC, are able to inhibit the canonical Wnt/β-catenin pathway (Bisson et al., 2015; Nemeth et al., 2007). In addition, we also identified PKCδ as a hub molecule linking ROR2 to ERK for mediation of WLS's function in NEPC, as shown by a Wnt-regulated phospho antibody array. PKCδ's controversial role in PC depends on the cellular context. PKCδ induces apoptosis in androgen-dependent PC cells via autocrine secretion of death factors, but has pro-survival effects in PC cells displaying stem cell properties, which are reported to be retained in NEPC cells as well (Gonzalez-Guerrico et al., 2005; Harris and Kerr, 2017; Kumar et al., 2014). Nevertheless, we showed that PKCδ is required for the maintenance of NE and the proliferative characteristics of NEPC cells. Our data collectively support the idea that WLS-Wnt signaling activation of the ROR2/PKCδ/ERK noncanonical Wnt pathway displaces the AR-dependent mechanism to promote the acquisition of an NE phenotype and confer growth advantages in NEPC cells.

In light of the complex transduction processes in the receiving cells, inhibition of Wnt ligand secretion in the producing cells has been considered one of the most efficacious ways to target Wnt signaling in cancer. The prevalent upregulation of Wnts and WLS in ENZ^R NEPC cells provides a rationale for using Wnt secretion inhibitors to treat NEPC. The orally bioavailable small-molecule inhibitor LGK974, which interferes with Wnt secretion by binding directly to and inhibiting PORCN, showed promise in an NEPC tumor xenograft mouse model in addition to *in vitro* settings. Notably, LGK974 treatment inhibited NEPC tumor growth as well as tumor expression of the NE marker CD56 much more drastically than the genetic silencing of WLS, which might be in large part due to global inhibition of Wnt secretion in mice including secretion by the mouse tumor microenvironment. LGK974 is currently being tested in a Phase I dose escalation clinical trial (NCT01351103) for patients with malignancies dependent on Wnt ligands. This multi-site trial is still in the recruiting phase for most of the sites participating in the trial but is currently active and set to be completed in 2022. The results of the interim analysis recently demonstrated that a combined use of LGK974 (named as WNT974 in this trial) ± spartalizumab alongside effective skin *AXIN2* suppression was well tolerated in patients with several types of advanced solid tumors (Janku et al., 2020). Nevertheless, more attention to the end results of this trial would be needed for an overall assessment of the safety and potential of LGK974 for further clinical development. In a recent study, LGK974 also demonstrated growth inhibition efficacy in CRPC-derived, AR-positive VCaP xenograft prostate tumors in mice, which could mirror a precursor of NEPC if coupled to API exposure (Ma et al., 2016). Whether LGK974 treatment could prevent the transition of CRPC into NEPC merits further investigation using a recently described serial transplantation xenograft model in the presence of ENZ (Bishop et al., 2017).

In conclusion, we demonstrated the functional importance of WLS for mediating the development and progression of NEPC under the selective pressures of APIs such as ENZ. We also provided strong preclinical evidence for using Wnt secretion inhibitors for a wide-spectrum inhibition of the Wnt pathway as a potential targeted therapy for NEPC.

Limitations of the study

This study would be strengthened by including more bona fide human NEPC cell lines to consolidate the major findings and also by using a more clinically relevant animal model, such as the NEPC patient-derived xenograft model, to evaluate LGK974's effectiveness for halting NEPC growth in mice.

Resource availability

Lead contact

Further information and requests for resources and reagents should be directed to and will be fulfilled by the lead contact, Boyang (Jason) Wu (boyang.wu@wsu.edu).

Materials availability

This study did not generate new unique reagents.

Data and code availability

The control and C4-2B^{ENZR} cell RNA-seq data generated during this study are available at GEO with the accession number GSE159548.

Methods

All methods can be found in the accompanying Transparent methods supplemental file.

Supplemental information

Supplemental information can be found online at https://doi.org/10.1016/j.isci.2020.101970.

Acknowledgments

This work was supported by NIH/NCI grant R37CA233658, Department of Defense Prostate Cancer Research Program grant W81XWH-19-1-0279, and WSU startup funds to B.J.W. We thank Yidi Xu (Washington State University) for providing technical assistance. We also thank Gary Mawyer for editorial assistance.

Authors contribution

T.B. and B.J.W. conceived and designed the study. T.B., J.W., L.Y., T.P., J.L., and J.G. performed the experiments. T.B., J.W., L.Y., and B.J.W. analyzed and interpreted the data. T-P.L. provide human CRPC specimens. A.C.G. provided control and ENZ^{R} C4-2B cells. T.B. and B.J.W. wrote the manuscript. B.J.W. supervised the overall research and acquired funding.

Declaration of interests

The authors declare no competing interests.

Received: April 27, 2020
Revised: November 12, 2020
Accepted: December 16, 2020
Published: January 22, 2021

References

Akamatsu, S., Wyatt, A.W., Lin, D., Lysakowski, S., Zhang, F., Kim, S., Tse, C., Wang, K., Mo, F., Haegert, A., et al. (2015). The placental gene PEG10 promotes progression of neuroendocrine prostate cancer. Cell Rep. *12*, 922–936.

Aparicio, A., Logothetis, C.J., and Maity, S.N. (2011). Understanding the lethal variant of prostate cancer: power of examining extremes. Cancer Discov. *1*, 466–468.

Augustin, I., Goidts, V., Bongers, A., Kerr, G., Vollert, G., Radlwimmer, B., Hartmann, C., Herold-Mende, C., Reifenberger, G., von Deimling, A., and Boutros, M. (2012). The Wnt secretion protein Evi/Gpr177 promotes glioma tumourigenesis. EMBO Mol. Med. *4*, 38–51.

Banziger, C., Soldini, D., Schutt, C., Zipperlen, P., Hausmann, G., and Basler, K. (2006). Wntless, a conserved membrane protein dedicated to the secretion of Wnt proteins from signaling cells. Cell *125*, 509–522.

Bartscherer, K., Pelte, N., Ingelfinger, D., and Boutros, M. (2006). Secretion of Wnt ligands requires Evi, a conserved transmembrane protein. Cell *125*, 523–533.

Beltran, H., Prandi, D., Mosquera, J.M., Benelli, M., Puca, L., Cyrta, J., Marotz, C., Giannopoulou, E., Chakravarthi, B.V., Varambally, S., et al. (2016). Divergent clonal evolution of castration-resistant neuroendocrine prostate cancer. Nat. Med. *22*, 298–305.

Beltran, H., Tomlins, S., Aparicio, A., Arora, V., Rickman, D., Ayala, G., Huang, J., True, L., Gleave, M.E., Soule, H., et al. (2014). Aggressive variants of castration-resistant prostate cancer. Clin. Cancer Res. *20*, 2846–2850.

Bishop, J.L., Thaper, D., Vahid, S., Davies, A., Ketola, K., Kuruma, H., Jama, R., Nip, K.M., Angeles, A., Johnson, F., et al. (2017). The master neural transcription factor BRN2 is an androgen receptor-suppressed driver of neuroendocrine differentiation in prostate cancer. Cancer Discov. *7*, 54–71.

Bisson, J.A., Mills, B., Paul Helt, J.C., Zwaka, T.P., and Cohen, E.D. (2015). Wnt5a and Wnt11 inhibit the canonical Wnt pathway and promote cardiac progenitor development via the Caspase-dependent degradation of AKT. Dev. Biol. *398*, 80–96.

Chen, X., Liu, J., Cheng, L., Li, C., Zhang, Z., Bai, Y., Wang, R., Han, T., Huang, C., Kong, Y., et al. (2020). Inhibition of noncanonical Wnt pathway overcomes enzalutamide resistance in castration-resistant prostate cancer. Prostate *80*, 256–266.

Chen, Y., Nowak, I., Huang, J., Keng, P.C., Sun, H., Xu, H., Wei, G., and Lee, S.O. (2014). Erk/MAP kinase signaling pathway and neuroendocrine differentiation of non-small-cell lung cancer. J. Thorac. Oncol. *9*, 50–58.

Cheung, R., Kelly, J., and Macleod, R.J. (2011). Regulation of villin by wnt5a/ror2 signaling in human intestinal cells. Front. Physiol. *2*, 58.

Fu, J., Jiang, M., Mirando, A.J., Yu, H.M., and Hsu, W. (2009). Reciprocal regulation of Wnt and Gpr177/mouse Wntless is required for embryonic axis formation. Proc. Natl. Acad. Sci. U S A *106*, 18598–18603.

Glaeser, K., Urban, M., Fenech, E., Voloshanenko, O., Kranz, D., Lari, F., Christianson, J.C., and Boutros, M. (2018). ERAD-dependent control of the Wnt secretory factor Evi. EMBO J. *37*, e97311.

Gonzalez-Guerrico, A.M., Meshki, J., Xiao, L., Benavides, F., Conti, C.J., and Kazanietz, M.G. (2005). Molecular mechanisms of protein kinase C-induced apoptosis in prostate cancer cells. J. Biochem. Mol. Biol. *38*, 639–645.

Goodman, R.M., Thombre, S., Firtina, Z., Gray, D., Betts, D., Roebuck, J., Spana, E.P., and Selva, E.M. (2006). Sprinter: a novel transmembrane protein required for Wg secretion and signaling. Development *133*, 4901–4911.

Guo, H., Ci, X., Ahmed, M., Hua, J.T., Soares, F., Lin, D., Puca, L., Vosoughi, A., Xue, H., Li, E., et al.

(2019). ONECUT2 is a driver of neuroendocrine prostate cancer. Nat. Commun. *10*, 278.

Harris, K.S., and Kerr, B.A. (2017). Prostate cancer stem cell markers drive progression, therapeutic resistance, and bone metastasis. Stem Cells Int. *2017*, 8629234.

Ho, H.Y., Susman, M.W., Bikoff, J.B., Ryu, Y.K., Jonas, A.M., Hu, L., Kuruvilla, R., and Greenberg, M.E. (2012). Wnt5a-Ror-Dishevelled signaling constitutes a core developmental pathway that controls tissue morphogenesis. Proc. Natl. Acad. Sci. U S A *109*, 4044–4051.

Huss, W.J., Gregory, C.W., and Smith, G.J. (2004). Neuroendocrine cell differentiation in the CWR22 human prostate cancer xenograft: association with tumor cell proliferation prior to recurrence. Prostate *60*, 91–97.

Isaacsson Velho, P., Fu, W., Wang, H., Mirkheshti, N., Qazi, F., Lima, F.A.S., Shaukat, F., Carducci, M.A., Denmeade, S.R., Paller, C.J., et al. (2020). Wnt-pathway activating mutations are associated with resistance to first-line abiraterone and enzalutamide in castration-resistant prostate cancer. Eur. Urol. *77*, 14–21.

Janku, F., de Vos, F., de Miguel, M., Forde, P., Ribas, A., Nagasaka, M., Argiles, G., Arance, A.M., Calvo, A., Giannakis, M., et al. (2020). Phase I study of WNT974 + spartalizumab in patients (pts) with advanced solid tumors. Cancer Res. *80*, Abstract nr CT034. https://cancerres.aacrjournals.org/content/80/16_Supplement/CT034.

Kim, J., Adam, R.M., and Freeman, M.R. (2002). Activation of the Erk mitogen-activated protein kinase pathway stimulates neuroendocrine differentiation in LNCaP cells independently of cell cycle withdrawal and STAT3 phosphorylation. Cancer Res. *62*, 1549–1554.

Kim, J., Jin, H., Zhao, J.C., Yang, Y.A., Li, Y., Yang, X., Dong, X., and Yu, J. (2017). FOXA1 inhibits prostate cancer neuroendocrine differentiation. Oncogene *36*, 4072–4080.

Komiya, Y., and Habas, R. (2008). Wnt signal transduction pathways. Organogenesis *4*, 68–75.

Kumar, D., Shankar, S., and Srivastava, R.K. (2014). Rottlerin induces autophagy and apoptosis in prostate cancer stem cells via PI3K/Akt/mTOR signaling pathway. Cancer Lett. *343*, 179–189.

Labrecque, M.P., Coleman, I.M., Brown, L.G., True, L.D., Kollath, L., Lakely, B., Nguyen, H.M., Yang, Y.C., da Costa, R.M.G., Kaipainen, A., et al. (2019). Molecular profiling stratifies diverse phenotypes of treatment-refractory metastatic castration-resistant prostate cancer. J. Clin. Invest. *129*, 4492–4505.

Lapuk, A.V., Wu, C., Wyatt, A.W., McPherson, A., McConeghy, B.J., Brahmbhatt, S., Mo, F., Zoubeidi, A., Anderson, S., Bell, R.H., et al. (2012). From sequence to molecular pathology, and a mechanism driving the neuroendocrine phenotype in prostate cancer. J. Pathol. *227*, 286–297.

Lee, G.T., Kwon, S.J., Kim, J., Kwon, Y.S., Lee, N., Hong, J.H., Jamieson, C., Kim, W.J., and Kim, I.Y. (2018a). WNT5A induces castration-resistant prostate cancer via CCL2 and tumour-infiltrating macrophages. Br. J. Cancer *118*, 670–678.

Lee, G.T., Rosenfeld, J.A., Kim, W.T., Kwon, Y.S., Palapattu, G., Mehra, R., Kim, W.J., and Kim, I.Y. (2019). TCF4 induces enzalutamide resistance via neuroendocrine differentiation in prostate cancer. PloS one *14*, e0213488.

Lee, Y.F., Lee, C.Y., Lai, L.C., Tsai, M.H., Lu, T.P., and Chuang, E.Y. (2018b). CellExpress: A Comprehensive Microarray-Based Cancer Cell Line and Clinical Sample Gene Expression Analysis Online System*2018* (Database).

Li, Y., Chan, S.C., Brand, L.J., Hwang, T.H., Silverstein, K.A., and Dehm, S.M. (2013). Androgen receptor splice variants mediate enzalutamide resistance in castration-resistant prostate cancer cell lines. Cancer Res. *73*, 483–489.

Liu, C., Lou, W., Yang, J.C., Liu, L., Armstrong, C.M., Lombard, A.P., Zhao, R., Noel, O.D.V., Tepper, C.G., Chen, H.W., et al. (2018). Proteostasis by STUB1/HSP70 complex controls sensitivity to androgen receptor targeted therapy in advanced prostate cancer. Nat. Commun. *9*, 4700.

Liu, C., Lou, W., Zhu, Y., Yang, J.C., Nadiminty, N., Gaikwad, N.W., Evans, C.P., and Gao, A.C. (2015). Intracrine androgens and AKR1C3 activation confer resistance to enzalutamide in prostate cancer. Cancer Res. *75*, 1413–1422.

Liu, J., Pan, S., Hsieh, M.H., Ng, N., Sun, F., Wang, T., Kasibhatla, S., Schuller, A.G., Li, A.G., Cheng, D., et al. (2013). Targeting wnt-driven cancer through the inhibition of porcupine by LGK974. Proc. Natl. Acad. Sci. U S A *110*, 20224–20229.

Lombard, A.P., Liu, C., Armstrong, C.M., D'Abronzo, L.S., Lou, W., Evans, C.P., and Gao, A.C. (2019). Wntless promotes cellular viability and resistance to enzalutamide in castration-resistant prostate cancer cells. Am. J. Clin. Exp. Urol. *7*, 203–214.

Ma, F., Ye, H., He, H.H., Gerrin, S.J., Chen, S., Tanenbaum, B.A., Cai, C., Sowalsky, A.G., He, L., Wang, H., et al. (2016). SOX9 drives WNT pathway activation in prostate cancer. J. Clin. Invest. *126*, 1745–1758.

Miyamoto, D.T., Zheng, Y., Wittner, B.S., Lee, R.J., Zhu, H., Broderick, K.T., Desai, R., Fox, D.B., Brannigan, B.W., Trautwein, J., et al. (2015). RNA-Seq of single prostate CTCs implicates noncanonical Wnt signaling in antiandrogen resistance. Science *349*, 1351–1356.

Moparthi, L., Pizzolato, G., and Koch, S. (2019). Wnt activator FOXB2 drives the neuroendocrine differentiation of prostate cancer. Proc. Natl. Acad. Sci. U S A *116*, 22189–22195.

Murillo-Garzon, V., and Kypta, R. (2017). WNT signalling in prostate cancer. Nat. Rev. Urol. *14*, 683–696.

Nemeth, M.J., Topol, L., Anderson, S.M., Yang, Y., and Bodine, D.M. (2007). Wnt5a inhibits canonical Wnt signaling in hematopoietic stem cells and enhances repopulation. Proc. Natl. Acad. Sci. U S A *104*, 15436–15441.

Qi, J., Nakayama, K., Cardiff, R.D., Borowsky, A.D., Kaul, K., Williams, R., Krajewski, S., Mercola, D., Carpenter, P.M., Bowtell, D., and Ronai, Z.A. (2010). Siah2-dependent concerted activity of HIF and FoxA2 regulates formation of neuroendocrine phenotype and neuroendocrine prostate tumors. Cancer Cell *18*, 23–38.

Ramadan, W.H., Kabbara, W.K., and Al Basiouni Al Masri, H.S. (2015). Enzalutamide for patients with metastatic castration-resistant prostate cancer. Onco Targets Ther. *8*, 871–876.

Ren, D., Dai, Y., Yang, Q., Zhang, X., Guo, W., Ye, L., Huang, S., Chen, X., Lai, Y., Du, H., et al. (2019). Wnt5a induces and maintains prostate cancer cells dormancy in bone. J. Exp. Med. *216*, 428–449.

Roche, P.J., Hoare, S.A., and Parker, M.G. (1992). A consensus DNA-binding site for the androgen receptor. Mol. Endocrinol. *6*, 2229–2235.

Schmid, S.C., Sathe, A., Guerth, F., Seitz, A.K., Heck, M.M., Maurer, T., Schwarzenbock, S.M., Krause, B.J., Schulz, W.A., Stoehr, R., et al. (2017). Wntless promotes bladder cancer growth and acts synergistically as a molecular target in combination with cisplatin. Urol. Oncol. *35*, 544.e1–544.e10.

Seo, J., Kee, H.J., Choi, H.J., Lee, J.E., Park, S.Y., Lee, S.H., Jeong, M.H., Guk, G., Lee, S., Choi, K.C., et al. (2018). Inhibition of Wntless/GPR177 suppresses gastric tumorigenesis. BMB Rep. *51*, 255–260.

Siegel, R.L., Miller, K.D., and Jemal, A. (2019). Cancer statistics, 2019. CA: Cancer J. Clin. *69*, 7–34.

Sramkoski, R.M., Pretlow, T.G., 2nd, Giaconia, J.M., Pretlow, T.P., Schwartz, S., Sy, M.S., Marengo, S.R., Rhim, J.S., Zhang, D., and Jacobberger, J.W. (1999). A new human prostate carcinoma cell line, 22Rv1. In Vitro Cell. Dev. Biol. Anim. *35*, 403–409.

Sternberg, C.N. (2019). Enzalutamide, an oral androgen receptor inhibitor for treatment of castration-resistant prostate cancer. Future Oncol. *15*, 1437–1457.

Tai, S., Sun, Y., Squires, J.M., Zhang, H., Oh, W.K., Liang, C.Z., and Huang, J. (2011). PC3 is a cell line characteristic of prostatic small cell carcinoma. Prostate *71*, 1668–1679.

Takashima, A., English, B., Chen, Z., Cao, J., Cui, R., Williams, R.M., and Faller, D.V. (2014). Protein kinase Cdelta is a therapeutic target in malignant melanoma with NRAS mutation. ACS Chem. Biol. *9*, 1003–1014.

Tamai, K., Zeng, X., Liu, C., Zhang, X., Harada, Y., Chang, Z., and He, X. (2004). A mechanism for Wnt coreceptor activation. Mol. Cel. *13*, 149–156.

Thiele, S., Zimmer, A., Gobel, A., Rachner, T.D., Rother, S., Fuessel, S., Froehner, M., Wirth, M.P., Muders, M.H., Baretton, G.B., et al. (2018). Role of WNT5A receptors FZD5 and RYK in prostate cancer cells. Oncotarget *9*, 27293–27304.

Ueda, Y., Hirai, S., Osada, S., Suzuki, A., Mizuno, K., and Ohno, S. (1996). Protein kinase C activates the MEK-ERK pathway in a manner independent of Ras and dependent on Raf. J. Biol. Chem. *271*, 23512–23519.

Uysal-Onganer, P., Kawano, Y., Caro, M., Walker, M.M., Diez, S., Darrington, R.S., Waxman, J., and Kypta, R.M. (2010). Wnt-11 promotes neuroendocrine-like differentiation, survival and

migration of prostate cancer cells. Mol. Cancer *9*, 55.

Wang, H.T., Yao, Y.H., Li, B.G., Tang, Y., Chang, J.W., and Zhang, J. (2014). Neuroendocrine Prostate Cancer (NEPC) progressing from conventional prostatic adenocarcinoma: factors associated with time to development of NEPC and survival from NEPC diagnosis-a systematic review and pooled analysis. J. Clin. Oncol. *32*, 3383–3390.

Wong, Y.N., Ferraldeschi, R., Attard, G., and de Bono, J. (2014). Evolution of androgen receptor targeted therapy for advanced prostate cancer. Nat. Rev. Clin. Oncol. *11*, 365–376.

Xu, Y., Ma, Y.H., Pang, Y.X., Zhao, Z., Lu, J.J., Mao, H.L., and Liu, P.S. (2017). Ectopic repression of receptor tyrosine kinase-like orphan receptor 2 inhibits malignant transformation of ovarian cancer cells by reversing epithelial-mesenchymal transition. Tumour Biol. *39*, 1010428317701627.

Yu, J., Chia, J., Canning, C.A., Jones, C.M., Bard, F.A., and Virshup, D.M. (2014). WLS retrograde transport to the endoplasmic reticulum during Wnt secretion. Dev. Cell *29*, 277–291.

Zhang, Z., Cheng, L., Li, J., Farah, E., Atallah, N.M., Pascuzzi, P.E., Gupta, S., and Liu, X. (2018). Inhibition of the wnt/beta-catenin pathway overcomes resistance to enzalutamide in castration-resistant prostate cancer. Cancer Res. *78*, 3147–3162.

iScience, Volume *24*

Supplemental Information

WLS-Wnt signaling promotes neuroendocrine prostate cancer

Tyler Bland, Jing Wang, Lijuan Yin, Tianjie Pu, Jingjing Li, Jin Gao, Tzu-Ping Lin, Allen C. Gao, and Boyang Jason Wu

Supplemental Information

WLS-Wnt Signaling Promotes Neuroendocrine Prostate Cancer

Tyler Bland, Jing Wang, Lijuan Yin, Tianjie Pu, Jingjing Li, Jin Gao, Tzu-Ping Lin, Allen C. Gao, and Boyang Jason Wu

TRANSPARENT METHODS

Tissue Microarrays (TMAs)

The hormone-sensitive prostate cancer (HSPC) TMA (n=39) was obtained from PC TMA PR483 (US Biomax) containing 39 cases of primary prostate adenocarcinoma with a single core and 1.5 mm diameter size. The castration-resistant prostate cancer (CRPC) TMA (n=21) was constructed by the Biobank of Taipei General Veterans Hospital. This study was reviewed and approved by the IRB of Taipei General Veterans Hospital, and written informed consent was provided for patients. This study utilizing de-identified clinical specimens from the tissue microarrays received prior exemption from the IRB of Washington State University.

Cell Culture

Human PC LNCaP, 22Rv1 and PC-3 cell lines were obtained from the American Type Culture Collection. The human C4-2B cell line was provided by Leland W.K. Chung (Cedars-Sinai Medical Center). The control and ENZ-resistant (ENZ^R) C4-2B ($C4\text{-}2B^{ENZR}$) cell lines were generated as described previously (Liu et al., 2015). All cells were regularly tested for *Mycoplasma* with the MycoProbe Mycoplasma Detection Kit (R&D Systems) and used with the number of cell passages below 15. All PC cells were cultured in RPMI-1640 media (Corning) supplemented with 10% fetal bovine serum (FBS, Atlanta Biologicals) and 1% penicillin/streptomycin (Corning). $C4\text{-}2B^{ENZR}$ cells were cultured in regular FBS-supplemented media further containing 20 μM ENZ to maintain resistance to ENZ (Liu et al., 2015). In the experiments in need of decreased AR signaling, cells were maintained in hormone-depleted media composed of phenol red-free RPMI-1640 media, 5% charcoal-stripped serum (CSS, Atlanta Biologicals) and 1% penicillin/streptomycin.

Plasmids, siRNAs and Reagents

The TOPFlash plasmid that encodes seven copies of LEF/TCF-binding sites linked to *Firefly* luciferase and reflects Wnt/β-catenin signaling activity, and the corresponding FOPFlash (TOPFlash mutant) plasmid were provided by Randall Moon (University of Washington) and obtained from Addgene. The p-SV-β-Galactosidase control vector plasmid was purchased from Promega. Human *AR*, *ROR2*, *PKCδ*, *ERK1/2*, and non-target control siRNAs were purchased from Santa Cruz, Origene or Horizon Discovery. Human ROR2 expression plasmid was purchased from SinoBiological. Enzalutamide (SelleckChem), R1881 (Sigma-Aldrich), LGK974 (AdooQ Bioscience), BJE-106 (Axon Medchem), and UO126 (ApexBio) were purchased from respective vendors. The recombinant human Wnt5A protein was purchased from R&D Systems.

Generation of Stable Knockdown (KD) cells

Stable shRNA-mediated WLS KD was achieved by infecting cells with lentiviral particles expressing *WLS* shRNA TRCN0000133858 (shWLS#1, mainly used in this study and also dubbed "shWLS") or TRCN0000133999 (shWLS#2), followed by 2-week puromycin selection (2 μg/ml) to establish stable cell lines. A non-target control shRNA (shCon) was used as control in stable KD cells. WLS KD was validated by Western blot.

Biochemical Analyses

Total RNA was isolated with Trizol (Thermo Fisher Scientific) and reverse-transcribed to cDNA by M-MLV reverse transcriptase (Promega) following the manufacturers' instructions. Subsequently, qPCR was conducted using SYBR Green PCR Master Mix and run with the Applied Biosystems QuantStudio 3 Real-Time PCR System (Thermo Fisher Scientific). PCR conditions included an initial denaturation step of 10 min at 95°C, followed by 40 cycles of PCR consisting of 15 s at 95°C and 1 min at 60°C. The PCR data were analyzed by $2^{-\Delta\Delta CT}$ method (Livak and Schmittgen, 2001). Details on the primers for qPCR are provided in the

Supplemental Table 1. For Western blots, cells were extracted with radioimmunoprecipitation assay buffer in the presence of a protease and phosphatase inhibitor cocktail (Thermo Fisher Scientific), and blots were performed as described previously (Chen et al., 2011) using primary antibodies against WLS, AR, PSA, CHGA, NSE, CD56, Wnt5A, Wnt11, p-LRP6, LRP6, β-catenin, histone H3, GAPDH, p-PKCδ, PKCδ, p-ERK, ERK, p-JNK, JNK, p-AKT, AKT, β-catenin, histone H3, GAPDH, ROR2 or β-actin. Details on the antibodies for Western blot, including RRIDs, are provided in Supplemental Table 2. Nuclear and cytoplasmic protein extraction was performed with NE-PER Nuclear and Cytoplasmic Extraction Reagents (Thermo Fisher Scientific) according to the manufacturer's protocol. Wnt target phosphoproteins were probed using a Wnt Signaling Phospho Antibody Array (Full Moon BioSystems) following the manufacturer's instructions.

Analyses of Cell Proliferation and Colony Formation

Proliferation assays of PC cells were performed by seeding cells into 96-well plates at a density of 10,000 cells/well. Cells were treated with drugs and live cells were stained with crystal violet at designated time intervals. Crystal violet taken up by cells was dissolved in methanol and optical density at 570 nm wavelength was measured with a Synergy Neo Microplate Reader (BioTek). Alternatively, the MTS assay (Promega) was also used to assess cell proliferation following the manufacturer's instructions. To determine the effects of PKCδ, ERK and ROR2 on cell proliferation, PC cells were seeded into 6-well plates and transfected with siRNAs against individual genes with Lipofectamine 2000 (Thermo Fisher Scientific) according to the manufacturer's protocol. Cells were stripped and replated 24 hrs after transfection and growth was monitored over an additional period of up to 5 days. To determine the effect of ROR2 on rescuing cell proliferation caused by WLS silencing, WLS-KD cells were transfected with a *ROR2* expression plasmid, followed by evaluation of cell proliferation over a monitoring period for 5 days. Colony formation assays were performed by seeding cells into a 6-well plate at a density of 1,000 cells/well. Cells were grown until visible colonies formed, and then stained with crystal violet. Colonies were imaged with a ChemiDoc Touch Imaging System (Bio-Rad) and the number of colonies containing ≥50 cells was enumerated with ImageJ software (NIH).

Wnt Secretion Detection

Wnt proteins were isolated with Blue Sepharose beads as previously described (Ross et al., 2014). Briefly, PC cells were seeded into 6-well plates at equal density and grown for 72 hrs. Equal volumes (2 ml) of conditioned media were collected and filtered through 0.22-μm syringe filters. To each sample, the following components were added: 1% (v/v) Triton X-100, 20 mM Tris-HCl, pH 7.5, 0.01% (w/v) NaN_3, and 50 μl Blue Sepharose 6 Fast Flow beads (GE Healthcare). Samples were rotated for 10 min at room temperature and washed three times with PBS, and Wnt proteins were then eluted with SDS loading buffer containing 50 nM DTT. Blue Sepharose-precipitated proteins were analyzed by Western blot.

Chromatin Immunoprecipitation (ChIP)-qPCR Assays

ChIP assays were used to determine the association of endogenous AR protein with two putative androgen response elements (AREs) within *WLS* genomic sequences in R1881-treated LNCaP cells by a SimpleChIP Enzymatic Chromatin IP Kit (Cell Signaling) following the manufacturer's instructions. Briefly, the chromatin was crosslinked with nuclear proteins, enzymatically digested with micrococcal nuclease followed by sonication, and immunoprecipitated with anti-AR (PG-21, Millipore) antibody. Normal IgG included in the kit was used as a negative control for IP. After being pelleted with agarose beads and purified, the immunoprecipitates were subjected to qPCR with two pairs of primers specifically targeting the *WLS* enhancer region encompassing the two AREs. Primer sequences for ARE1 are forward 5'-AACACTGTTGCTGTTTGATAGAAA-3' and reverse 5'-GAAGCATTTACTGGAACACTTGA-3'.

Primer sequences for ARE2 are forward 5'-TTGCCATAGTGTCTGCCTTG-3' and reverse 5'-CAGGGAAGTGGTTTGAGGAA-3'. Two percent of chromatin prior to IP was saved as input.

TOPFlash/FOPFlash Assay

PC cells were seeded into 12-well plates and transfected with the TOPFlash or FOPFlash plasmid expressing *Firefly* luciferase along with the p-SV-β-Galactosidase plasmid expressing β-galactosidase as internal control. Cells were harvested, and cell lysates were assayed for luciferase and β-galactosidase activities by the Luciferase Assay System (Promega) and the β-Galactosidase Enzyme Assay System (Promega) respectively according to the manufacturer's instructions. Relative TOPFlash or FOPFlash activities were determined by respective luciferase activity normalized to β-galactosidase activity. The TOPFlash/FOPFlash ratios were calculated to reflect Wnt/ β-catenin signaling activity.

Animal Studies

All animal studies received prior approval from the IACUC of Washington State University and complied with IACUC recommendations. Male 6-week-old SCID mice or athymic nude mice were purchased from Charles River or the Jackson Laboratory, housed in the animal research facility at Washington State University, and fed with a sterile normal chow diet. For determining the effect of WLS on tumor growth, 3 x 10^6 22Rv1 (control and WLS KD) cells were mixed 1:1 with Matrigel (BD Biosciences) and injected subcutaneously into the flank of castrated SCID mice. Tumor size was measured three times per week by caliper from the time of formation of palpable tumors. Tumor volume was calculated by the formula of length x width^2 x 0.52. After 3 weeks, the mice were sacrificed and tumors were weighed and collected for immunohistochemical (IHC) analyses. For determining the effect of LGK974 on tumor growth, 3 x 10^6 22Rv1 cells were mixed 1:1 with Matrigel and subcutaneously implanted into the flank of castrated nude mice. Once palpable tumors formed, mice were randomly assigned into two groups to receive respective treatments: vehicle (corn oil, oral gavage, daily) and LGK974 (5mg/kg, oral gavage, daily). Tumor size was measured three times per week. After 3 weeks or after the tumor diameter reached 20 mm, the mice were sacrificed, and tumors were weighed and collected for IHC analyses.

IHC Analysis

IHC analysis of clinical and xenograft tumor samples was performed as described previously (Li et al., 2020) using antibodies against WLS, CHGA, Ki-67, cleaved caspase 3, CD34, CD56, p-PKCδ or p-ERK. Details on the antibodies for IHC, including RRIDs, are provided in Supplemental Table 2. Cell-based averages of staining intensity for WLS and CHGA in clinical samples were analyzed by inForm software (PerkinElmer), an automated image analysis software enabling per-cell analysis of stained samples, after areas of interest were defined using manual tissue segmentation by a pathologist. IHC staining of WLS, Ki-67, cleaved caspase 3, CD34, CD56, p-PKCδ and p-ERK in xenograft tumor samples were quantified with ImageJ.

RNA-seq and Gene Set Enrichment Analysis (GSEA)

The total RNA of control and ENZ^R C4-2B cells was extracted by RNeasy Mini Kit (Qiagen) following the manufacturer's instructions. RNA-seq was performed on an Illumina HiSeq 2500 at UCLA Clinical Microarray Core. Bowtie 2 v2.1.0 was used for mapping to the human genome hg19 transcript set. RSEM v1.2.15 was used to calculate the count and estimate the gene expression level. Trimmed Mean of M-values (TMM) method in the edgeR package was used for gene expression normalization. The RNA-seq raw sequence files reported in this manuscript have been submitted to the NCBI Gene Expression Omnibus database (accession no. GSE159548). GSEA v4.0.3 was used to evaluate the association of ENZ resistance with

androgenic, neuronal or Wnt pathways using relevant gene sets from the molecular signature database (MSigDB v7.2).

Bioinformatic Analysis

The human PC datasets used for gene co-expression correlative studies or examination of *WLS* and ROR2 gene expression were downloaded from the cBioPortal for Cancer Genomics database or the NCBI Gene Expression Omnibus database. For analyzing ChIP-seq datasets GSE55062 and GSE70079 available in Gene Expression Omnibus database, Bowtie was used to map the human hg19 genome and unique mapped reads were used for peak calling. MACS2 was used to perform the peak calling and ChIPseeker was used for peak annotation.

Statistics

All experiments were performed in triplicate and repeated at least 3 times. All data are expressed as the mean ± SEM. Multiple comparisons were analyzed using one-way ANOVA with post-hoc Tukey's analysis and single comparisons were analyzed using a two-tailed, unpaired Student's *t* test. Correlations were determined by Pearson correlation. Statistical significance was set to a minimum of $p<0.05$.

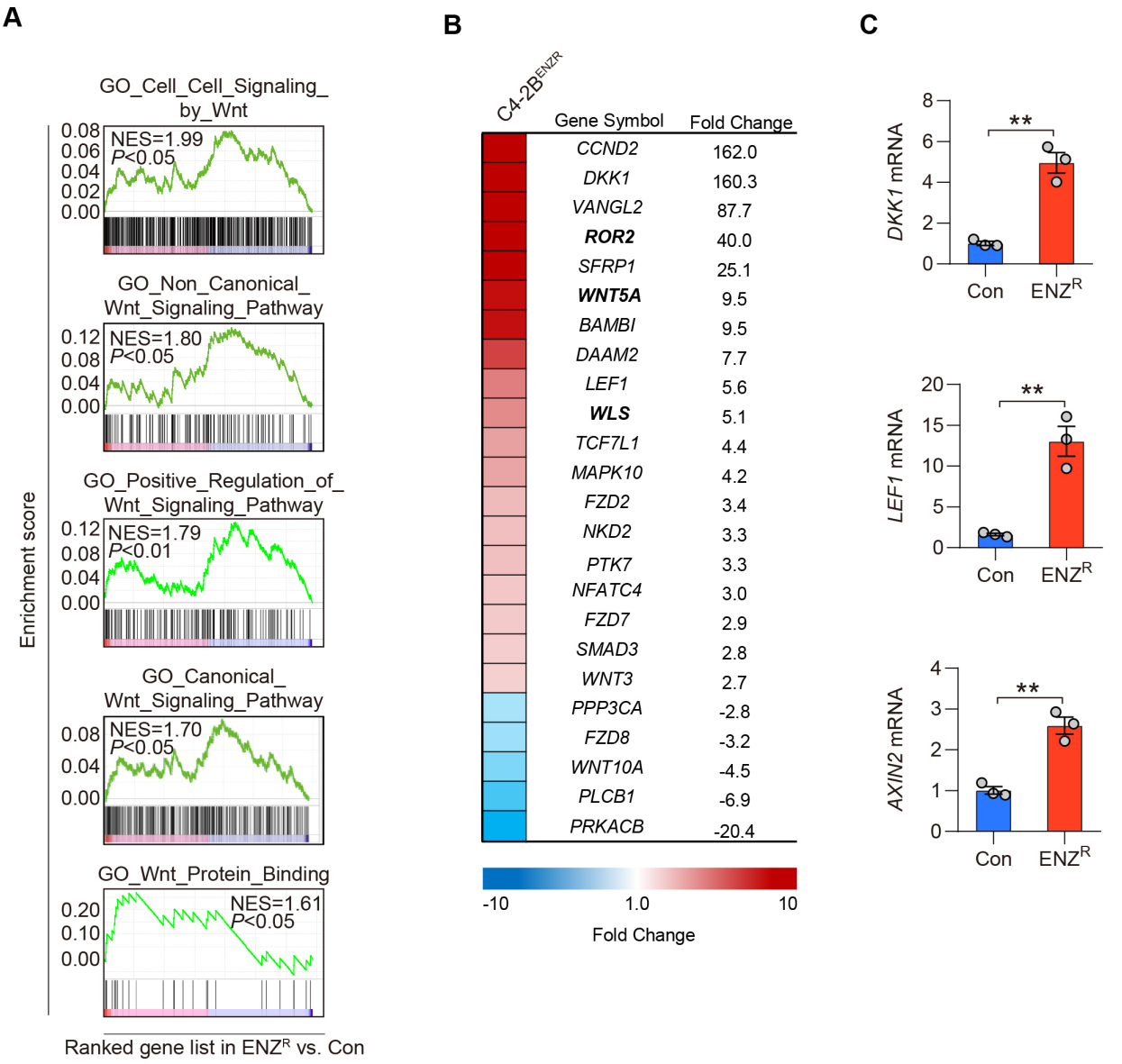

Figure S1. Wnt Signaling Is Activated in ENZ^R NEPC Cells, Related to Figure 1.
(A) GSEA plots of positive enrichment of gene sets related to Wnt signaling in ENZ^R C4-2B cells compared to ENZ-sensitive control C4-2B cells.
(B) The heat map depicts the fold change of mRNA levels of Wnt pathway-related genes in ENZ^R C4-2B (C4-2B^{ENZR}) cells compared to controls. *WLS*, *ROR2* and *Wnt5A* are highlighted in bold for emphasis.
(C) RT-qPCR analysis of mRNA levels of select target genes of the canonical Wnt pathway in control and C4-2B^{ENZR} cells (n=3). Data represent the mean ± SEM. ***p*<0.01, unpaired *t* test.

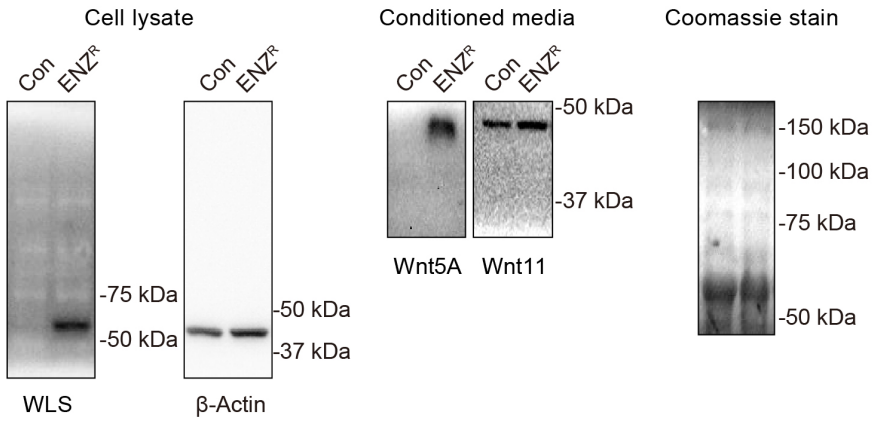

Figure S2. WLS and Wnt Protein Expression Are Upregulated in ENZ^{R} NEPC Cells, Related to Figure 1.

Western blot analysis of WLS protein expression in cell lysates and secreted Wnt5A and Wnt11 protein levels in conditioned media of control and C4-2B^{ENZR} cells. β-Actin was probed in cell lysates as loading control for WLS. Total proteins of conditioned media were visualized by Coomassie stain for normalizing Wnt5A and Wnt11 secreted in conditioned media. The complete uncropped blots are shown.

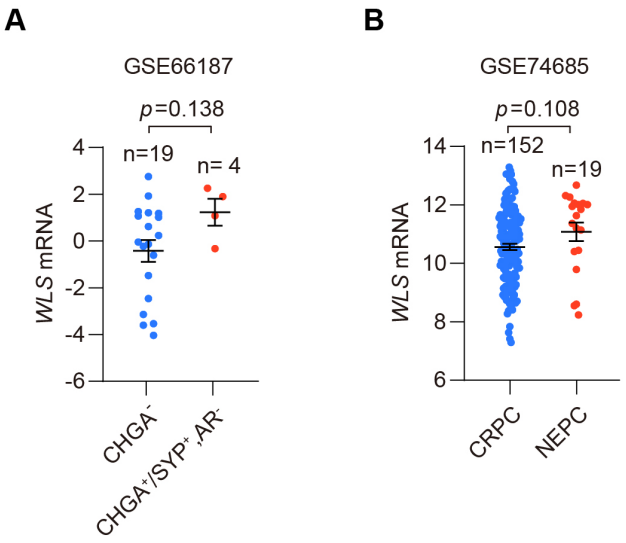

Figure S3. WLS Expression Exhibits an Increasing Trend in NEPC Relative to CRPC, Related to Figure 2.

(A and B) Quantification of *WLS* mRNA expression between CRPC and NEPC cohorts in 2 independent datasets, GSE66187 (A) and GSE74685 (B). Data represent the mean ± SEM. Unpaired *t* test.

A

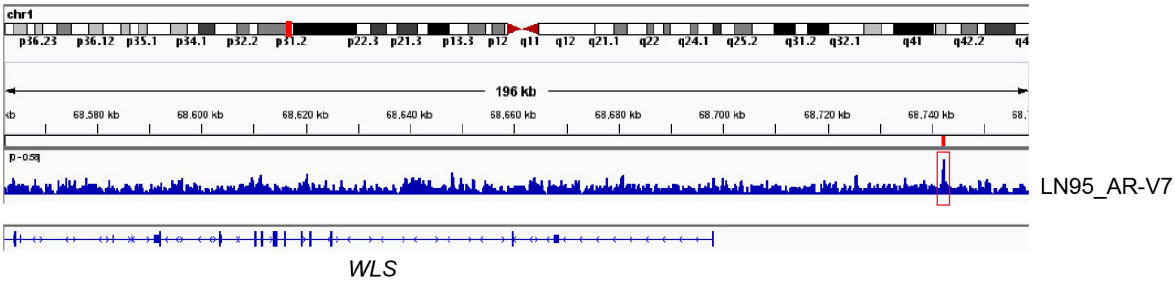

B

ACTCAGTCCTTTTGGCTTTCAAAGTAGGTCTCAGCAAAGGAAGACGCAAGCTACTGGTTTAGGATTAAACCTGGG
GAATCAGACTGGTCTGGACACTTGGTTTGCCAAGAGGCCTGGTAGTGGAGAATTCTGTGACTGGCAAATGCCTA
GGAGGCAAAGGAGTGAAAGTCTTGAGTTCTGAGAGAGACAACCTTTGGGTTCCTTAGGCACTAGGCAGTGGCCC
AAGGCACTGGGATCTTATGTAAATGGCAGAGCGCCCCAGGAGCTTCAGGTATGCTTATCTGCTCATCTAATGGAG
CCAAGGAGACAATCTGTTTAGATAACAGGTTGCAAGAGATAATGGACTCTGCTGGGAATGGCATGTTCCCTCCTG
GGGGGTAACCCTTAGATCTTGGAATTTGGCTGAGAGAAGGAGGCAATGCATGGTGCTCCTGCAGAGGTCTGAAA
AACAGCTGTGGAGTGCCTCACATGGTTTTCATCATGGCCTGAAAGTGTTCTCTCTCTCCATTGCCCGCCCCACCC
CCCAACCCATTTACTCTAAAAGTAAAAATAAATATGTTAAATATTTTGGAACCACCCACTAAATAGTAATTATAGATG
GTAGTAACTAATTACACTATTATCTATCACTTTT

Figure S4. Mapping AR-V7 Binding at *WLS* Gene Locus, Related to Figure 3.
(A) Genomic browser representation of AR-V7 binding in the *WLS* genomic sequences in LN95 cells from the ChIP-seq dataset GSE106559. The most outstanding track representing potential AR-V7 occupancy is highlighted in a rectangle of red borders.
(B) The sequences of AR-V7-enriched region identified from (A).

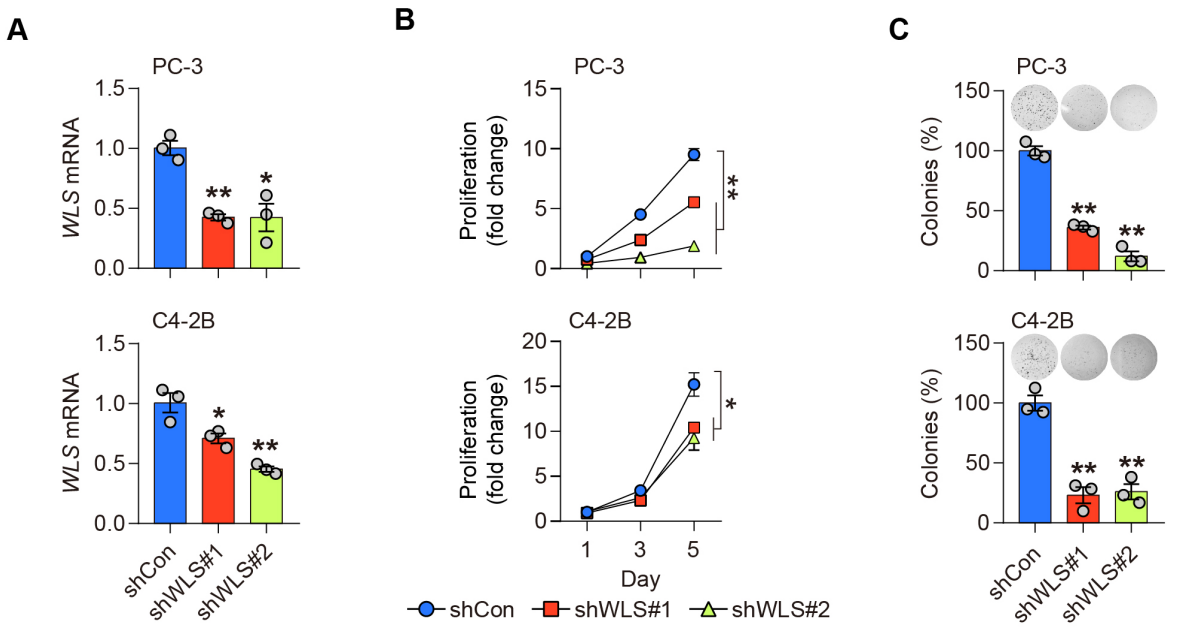

Figure S5. WLS Silencing Represses PC Cell Growth Independent of NE State, Related to Figure 4.

(A) RT-qPCR analysis of *WLS* mRNA expression in control and WLS-KD PC-3 and C4-2B cells (n=3). Data represent the mean ± SEM. **p*<0.05, ***p*<0.01, unpaired *t* test.

(B) Proliferation curves of control and WLS-KD PC-3 and C4-2B cells by crystal violet staining (n=4). Data represent the mean ± SEM. **p*<0.05, ***p*<0.01, one-way ANOVA.

(C) Colony formation assays of control and WLS-KD PC-3 and C4-2B cells (n=3) with the number of colonies in respective control groups set as 100%. Representative images from each group are shown. Data represent the mean ± SEM. ***p*<0.01, one-way ANOVA.

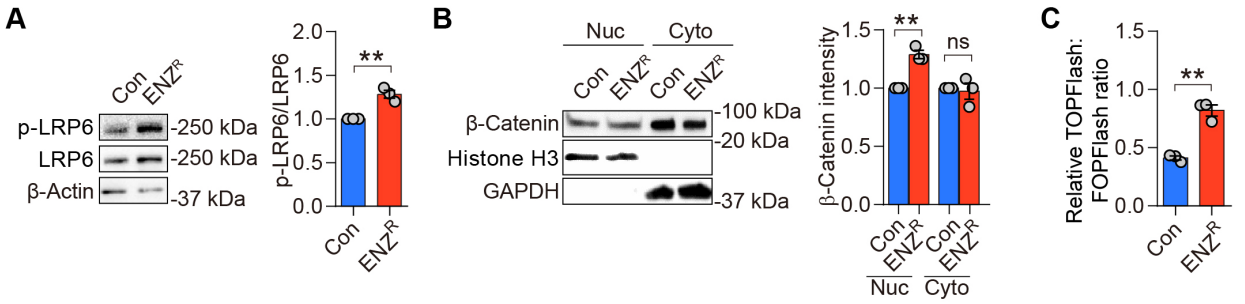

Figure S6. Canonical Wnt/β-Catenin Signaling Is Slightly Increased in ENZ^{R} NEPC Cells, Related to Figure 5.

(A) Western blot analysis of p-LRP6 and LRP6 protein expression in control and C4-2B^{ENZR} cells, with quantification of normalized p-LRP6 level presented separately (n=3). Data represent the mean ± SEM. ***p*<0.01, unpaired *t* test.

(B) Western blot analysis of β-catenin protein expression in nuclear (Nuc) and cytoplasmic (Cyto) extracts from control and C4-2B^{ENZR} cells, with quantification of nuclear and cytoplasmic β-catenin levels normalized to histone H3 and GAPDH respectively presented separately (n=3). Data represent the mean ± SEM. ***p*<0.01, ns, not significant, unpaired *t* test.

(C) Determination of Wnt/β-catenin signaling activity in control and C4-2B^{ENZR} cells by TOPFlash/FOPFlash assays. Relative TOPFlash or FOPFlash luciferase activities were determined by TOPflash or FOPFlash *Firefly* luciferase activity normalized to β-galactosidase activity expressed by the pSV-β-Galactosidase plasmid as internal control. The TOPFlash/FOPFlash ratios from each group are shown (n=3). Data represent the mean ± SEM. ***p*<0.01, unpaired *t* test.

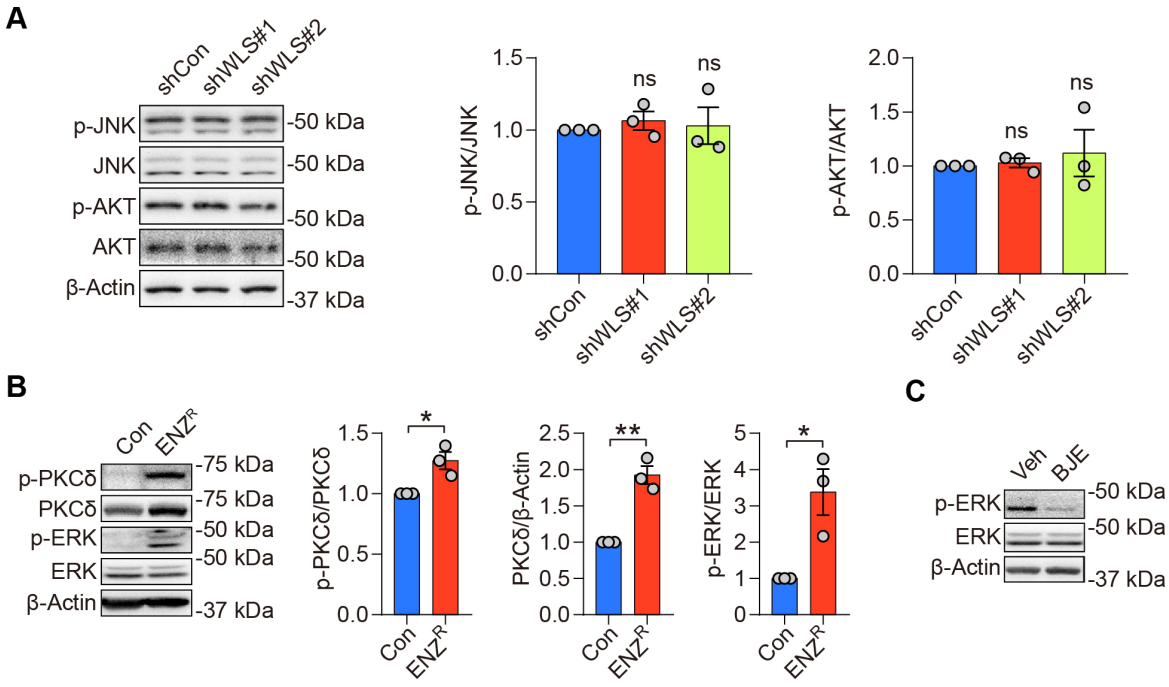

Figure S7. Phosphorylation of PKCδ and ERK but Not JNK and AKT Are Induced in ENZ^{R} NEPC cells, Related to Figure 5.

(A) Western blot analysis of p-JNK, JNK, p-AKT and AKT protein expression in control and C4-2B^{ENZR} cells, with quantification of normalized p-JNK and p-AKT levels presented separately (n=3). Data represent the mean ± SEM. ns, not significant, unpaired *t* test.

(B) Western blot analysis of p-PKCδ, PKCδ, p-ERK and ERK protein expression in control and C4-2B^{ENZR} cells, with quantification of normalized p-PKCδ, PKCδ and p-ERK levels presented separately. Data represent the mean ± SEM. **p*<0.05, ***p*<0.01, unpaired *t* test.

(C) Western blot analysis of p-ERK protein expression in C4-2B^{ENZR} cells treated with BJE-106 (0.1 μM, 3 hrs).

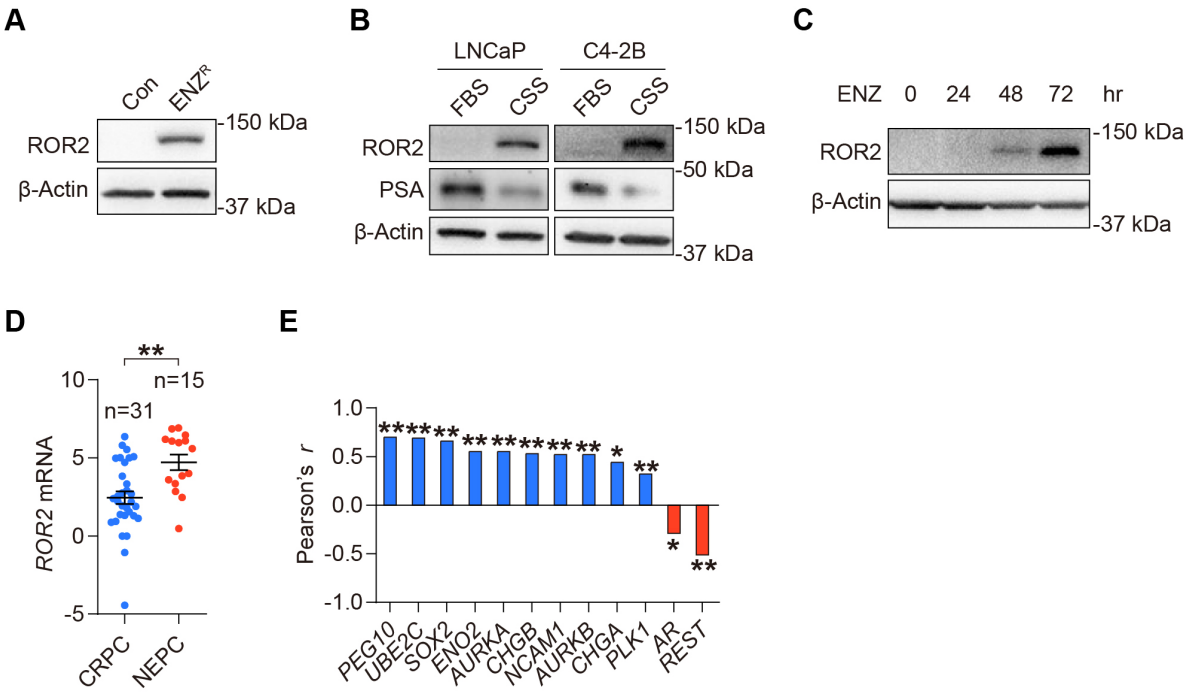

Figure S8. ROR2 Is Upregulated in ENZ^{R} NEPC Cells and Highly Expressed in Human NEPC, Related to Figure 6.

(A) Western blot analysis of ROR2 protein expression in control and C4-2B^{ENZR} cells.

(B) Western blot analysis of ROR2 and PSA protein expression in LNCaP and C4-2B cells grown in normal growth media (FBS) or CSS media for 5 days.

(C) Western blot analysis of ROR2 protein expression in LNCaP cells treated with 20 μM ENZ for different times.

(D) Quantification of *WLS* mRNA levels between CRPC (n = 31) and NEPC (n=15) cohorts in the Beltran dataset. Data represent the mean ± SEM. ***p*<0.01, unpaired *t* test.

(E) mRNA co-expression correlation of *ROR2* with NE marker genes, *REST* and *AR* represented by positive (blue) or inverse (red) correlations in the Beltran dataset. **p*<0.05, ***p*<0.01, Pearson correlation.

Gene	Forward	Reverse
WLS	TCCCTGGCTTACCGTGATGA	GCATTTGAGTTTCCGTGGTACT
DKK1	ATAGCACCTTGGATGGGTATTCC	CTGATGACCGGAGACAAACAG
LEF1	AGAACACCCCGATGACGGA	GGCATCATTATGTACCCGGAAT
AXIN2	AGAGCAGCTCAGCAAAAAGG	CCTTCATACATCGGGAGCAC
WNT1	TCCTCCACGAACCTGCTTAC	CGGATTTTGGCGTATCAGAC
WNT2B	CAAAGGTACATTGGGGCACT	ACTGAACGCATGATGTCTGG
WNT3	CCTTCACACCCACGAGGTTG	GACACTAACACGCCGAAGTCA
WNT3A	CTTTGCAGTGACACGCTCAT	GACACCATCCCACCAAACTC
WNT4	AGGAGGAGACGTGCGAGAAA	CGAGTCCATGACTTCCAGGT
WNT5A	GGACCACATGCAGTACATCG	CCTGCCAAAAACAGAGGTGT
WNT5B	GCTTCTGACAGACGCCAACT	CACCGATGATAAACATCTCGGG
WNT6	GGCAGCCCCTTGGTTATGG	CTCAGCCTGGCACAACTCG
WNT7A	CTGTGGCTGCGACAAAGAGAA	GCCGTGGCACTTACATTCC
WNT7B	GAAGCAGGGCTACTACAACCA	CGGCCTCATTGTTATGCAGGT
WNT8B	CCGACACCTTTCGCTCCATC	CAGCCCTAGCGTTTTGTTCTC
WNT9A	AGCAGCAAGTTCGTCAAGGAA	CCTTCACACCCACGAGGTTG
WNT9B	TGTGCGGTGACAACCTCAAG	ACAGGAGCCTGATACGCCAT
WNT10B	CATCCAGGCACGAATGCGA	CGGTTGTGGGTATCAATGAAGA
WNT11	GGAGTCGGCCTTCGTGTATG	GCCCGTAGCTGAGGTTGTC
GAPDH	GACAACAGCCTCAAGATCATCAG	ATGGCATGGACTGTGGTCATGAG

Table S1. Sequences of the Primers Used for RT-qPCR, Related to Figure 1.

Antibody	Source	Catalog #	RRID	Assay(s)
Goat anti-PSA (C-19)	Santa Cruz	sc-7638	AB_2134513	WB
Mouse anti-CHGA (C-12)	Santa Cruz	sc-393941	AB_2801371	WB and IHC
Mouse anti-NSE (NSE-P1)	Santa Cruz	sc-21738	AB_627513	WB
Mouse anti-β-Actin (AC-15)	Santa Cruz	sc-69879	AB_1119529	WB
Mouse anti-WLS (YJ5)	Millipore	MABS87	AB_11203675	WB
Rabbit anti-WLS	Proteintech	17950-1-AP	AB_2034928	IHC
Goat anti-Wnt5A	R&D	AF645	AB_2288488	WB
Mouse anti-Wnt5A (3A4)	Abnova	H00007474-M04	AB_1717123	IHC
Goat anti-Wnt11	R&D	AF2647	AB_2215119	WB
Mouse anti-AR (441)	Santa Cruz	sc-7305	AB_626671	WB
Mouse anti-AR (PG-21)	Millipore	06-680	AB_310214	ChIP
Mouse anti-CD56 (123C3)	Santa Cruz	sc-7326	AB_627127	WB and IHC
Rabbit anti-p-PKCδ (Tyr313)	CST	2055	AB_330876	WB and IHC
Rabbit anti-PKCδ (D10E2)	CST	9616	AB_10949973	WB
Mouse anti-p-ERK (E-4)	Santa Cruz	sc-7383	AB_627545	WB and IHC
Mouse anti-ERK (C-9)	Santa Cruz	sc-514302	AB_2571739	WB
Rabbit anti-p-LRP6 (Ser1490)	CST	2568	AB_1523898	WB
Rabbit anti-LRP6 (C47E12)	CST	3395	AB_1950408	WB
Rabbit anti-β-Catenin (D10A8)	CST	8480	AB_2798305	WB
Rabbit anti-Histone H3 (D1H2)	CST	4499	AB_10544537	WB
Mouse anti-GAPDH (0411)	Santa Cruz	sc-47724	AB_627678	WB
Rabbit anti-p-JNK (Thr183/Tyr185) (81E11)	CST	4668	AB_823588	WB
Rabbit anti-JNK	CST	9252	AB_2250373	WB
Rabbit anti-p-AKT (Ser124)	Cepham Life Sciences	14046	AB_2315049	WB
Rabbit anti-AKT (C67E7)	CST	4691	AB_915783	WB
Mouse anti-ROR2 (H-1)	Santa Cruz	sc-374174	AB_10989358	WB
Rabbit anti-Ki-67 (D2H10)	CST	9027	AB_2636984	IHC
Rabbit anti-Cleaved Caspase 3 (Asp175)	CST	9661	AB_2341188	IHC
Rabbit anti-CD34 (MCE 14.7)	Abcam	ab8158	AB_306316	IHC

Table S2. Antibodies Used, Related to Figures 1-7.

REFERENCES

Chen, K., Ou, X. M., Wu, J. B., and Shih, J. C. (2011). Transcription factor E2F-associated phosphoprotein (EAPP), RAM2/CDCA7L/JPO2 (R1), and simian virus 40 promoter factor 1 (Sp1) cooperatively regulate glucocorticoid activation of monoamine oxidase B. Molecular pharmacology *79*, 308-317.

Li, J., Pu, T., Yin, L., Li, Q., Liao, C. P., and Wu, B. J. (2020). MAOA-mediated reprogramming of stromal fibroblasts promotes prostate tumorigenesis and cancer stemness. Oncogene *39*, 3305-3321.

Liu, C., Lou, W., Zhu, Y., Yang, J. C., Nadiminty, N., Gaikwad, N. W., Evans, C. P., and Gao, A. C. (2015). Intracrine Androgens and AKR1C3 Activation Confer Resistance to Enzalutamide in Prostate Cancer. Cancer research *75*, 1413-1422.

Livak, K. J., and Schmittgen, T. D. (2001). Analysis of relative gene expression data using real-time quantitative PCR and the 2(-Delta Delta C(T)) Method. Methods *25*, 402-408.

Ross, J., Busch, J., Mintz, E., Ng, D., Stanley, A., Brafman, D., Sutton, V. R., Van den Veyver, I., and Willert, K. (2014). A rare human syndrome provides genetic evidence that WNT signaling is required for reprogramming of fibroblasts to induced pluripotent stem cells. Cell Rep *9*, 1770-1780.